

This is the **accepted version** of the journal article:

Reyes-Mateo, Kevin; Marquet, Jordi; Hernando, Jordi; [et al.]. «Photothermal polymerization of benzoxazines». Polymer Chemistry, Vol. 13, Issue 36 (September 2022), p. 5256-5264. DOI 10.1039/D2PY00635A

This version is available at <https://ddd.uab.cat/record/267122>

under the terms of the  **IN**
COPYRIGHT license

ARTICLE

Photothermal polymerization of benzoxazines

Kevin Reyes-Mateo,^a Jordi Marquet,^a Jordi Hernando*,^a and Rosa M. Sebastián*,^aReceived 00th January 20xx,
Accepted 00th January 20xx

DOI: 10.1039/x0xx00000x

Despite the use of catalysts and initiators, high polymerization temperatures are typically required for polybenzoxazines, a severe constraint for their general application as high performance thermosets. In this work we pioneer a novel photothermal strategy for the synthesis of polybenzoxazines that takes place under light irradiation at ambient conditions. This method capitalizes on the intriguing optical properties of benzoxazine-catalyst systems, which show visible light absorption and locally generate large heat upon illumination that triggers polymerization. In this way a large variety of benzoxazine monomers can be converted into polymer materials that retain some of the relevant features of polybenzoxazines – e.g., high char yields. In addition, our photothermal approach allows spatial control of benzoxazine polymerization, which we exploit for the fabrication of polybenzoxazine patterns via photolithography.

Introduction

A vast number of polymers are synthesized and processed at high temperatures,¹ an energy-intensive strategy that might eventually compromise their mass production and use. Photopolymerization emerges as a much-desired, environmentally-friendly alternative in those cases, which should not only allow reducing the energy demand for polymer formation but also grant direct access to a variety of materials under ambient conditions through advanced fabrication techniques— e.g., photolithography^{2,3} and 3D printing.^{4,5} A class of polymers that would largely benefit from these features are polybenzoxazines (PBz),^{6,7} a distinctive type of phenolic resins that are attracting much attention from industry because of their superior properties relative to traditional thermosets – e.g., near-zero volume change upon polymerization,^{8–10} low surface energy,¹¹ and high chemical resistance¹² and char yields,¹³ among others.^{14–16} Although PBz precursors – i.e., 1,3-benzoxazines (Bz) – can be readily prepared from low-cost and commercially available reagents, their ring-opening polymerization (ROP) is extremely energy demanding, as it takes place at particularly high temperatures ($T_p > 180$ °C).^{6,15} This is therefore a critical obstacle that precludes the widespread application of PBz.

Several approaches have so far been explored to decrease the polymerization temperature of PBz.¹⁷ On the one hand, we and others have investigated the use of initiators and catalysts for this purpose – e.g., Brønsted^{18,19} and Lewis acids –,^{20–24} which can be either added as separate components to the polymerization mixture^{18–24} or directly incorporated into the Bz monomers in a latent state.^{25–28} However, only moderate T_p reduction has been accomplished in this way for conventional monofunctional benzoxazines, although the introduction of additional functionalities may further lower the onset reaction temperature.^{20,29–31} Alternatively, Bz photopolymerization at room

temperature has been explored, though with limited results. For instance, Yagci and co-workers targeted this goal using onium salts as photoinitiators under UV irradiation. Unfortunately, only complex, low molecular weight polymer structures were obtained due to incomplete polymerization,³² which makes this strategy better suited for the cross-linking of main chain polybenzoxazine precursors.³³ Similarly, we could merely report low polymerization degrees for the photochemical ring-opening polymerization of Bz in water under direct UV photoexcitation, which was even inhibited for monomers bearing electron-withdrawing substituents.³⁴

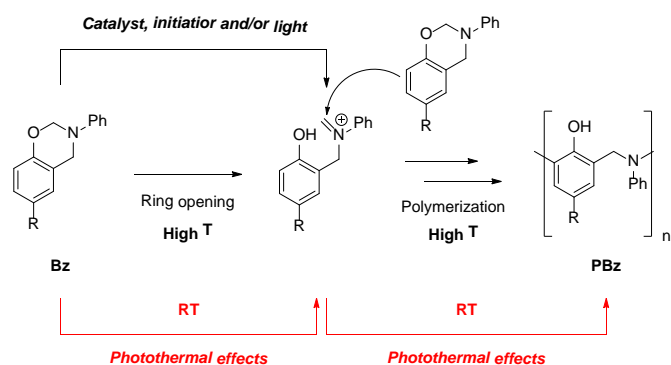
The reason why all these strategies fail to ensure the efficient production of PBz at low temperatures can be ascribed to their particular polymerization mechanism: while the initial ring-opening step of the monomers can be facilitated by initiators, catalysts and/or light, the subsequent electrophilic aromatic substitution reactions needed for extensive polymer network growth still require high thermal energy (Scheme 1).¹⁷ Herein we propose to circumvent this obstacle by means of a photothermal approach, where local heat is generated *in situ* under irradiation by relaxation of light absorbing species through electron-phonon interaction.^{35,36} Interestingly, this would allow complying with the high temperature demand of Bz polymerization without the need of external heating, while concomitantly benefitting from the inherent advantages of light-induced processes – i.e., precise time and space control over chemical reactivity (Scheme 1).

To date a narrow range of photothermally-induced polymerization processes have been described,^{37,38} which mainly comprise the photothermal curing of polysiloxanes,^{39–41} the photothermal initiation of acrylate polymerization^{42–52} and the photothermal polymerization of polyurethanes.^{53,54} In all these cases, reactions are promoted photothermally that take place at relatively moderate temperatures ($T < 100$ °C), while the aid of external photothermal agents is required that eventually lie entrapped in the final material – e.g., metal nanostructures,^{37–43,53,54} carbon (nano)materials^{44,46,48,51} or organic dyes,^{45,47,49,50} which are responsible for light absorption and heat generation. In contrast

^a Departament de Química, Universitat Autònoma de Barcelona, 08193, Cerdanyola del Vallès, Barcelona, Spain.

Email: jordi.hernando@uab.cat, rosamaria.sebastian@uab.es

†Electronic supplementary information (ESI) available: Materials and methods and further experimental data (NMR spectra, UV-vis absorption spectra, DSC and TGA thermograms). See DOI: XXXXXXXXXXXXXXXX



with these precedents, in this work we aim to (a) explore the more demanding photothermal polymerization of benzoxazines, which typically takes place at much higher temperatures, and (b) avoid the use of additional photoabsorbers. Instead, we intend to capitalize on the intriguing optical properties of Bz-catalyst systems, thus reducing the cost and complexity of the process.

Results and discussion

Photothermal properties of benzoxazine-catalyst systems

To test our photothermal strategy toward benzoxazine polymerization, a variety of previously reported Bz monomers were synthesized: several 1,3-benzoxazines bearing electron-donating and electron-withdrawing substituents (**Bz1-Bz8**)^{34,55-59} and bisbenzoxazine **Bz9**⁶⁰ (Fig. 1). Most monofunctional Bz were prepared through a solvent-free Mannich-type reaction by mixing 1,3,5-triphenyl-1,3,5-triazine or methylamine, paraformaldehyde and the respective phenol (**Bz1-Bz5**, **Bz7**). In the case of **Bz6** and **Bz8**, 1,4-dioxane also had to be added as a solvent to avoid concomitant thermal polymerization of the monomer formed. For bisbenzoxazine **Bz9**, the Mannich-type reaction was conducted using aniline, paraformaldehyde and bisphenol A as a bifunctional phenol. All monomers were isolated as white or slightly yellow solids, except for **Bz3** that was obtained as an orangish oil.

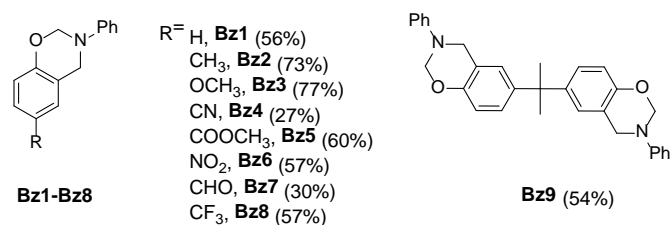


Fig. 1 Benzoxazine monomers synthesized via a Mannich-type reaction between an amine, formaldehyde and the corresponding phenol. Yields are shown in parentheses (see Table S1 and S2 in the ESI† for further details).

As expected, none of the benzoxazines synthesized showed significant absorbance in the visible region when investigated by UV-vis absorption spectroscopy in organic solution (Fig. 2a). Instead, they presented defined absorption bands in the UV spectrum with maxima at $\lambda_{\text{abs}} < 325$ nm. Consequently, they cannot be used as direct photoabsorbers of visible light to promote photothermal effects. Interestingly, a dramatic change in optical properties was observed upon addition of Lil, a metal salt previously identified by us as one of the most efficient catalysts of Bz polymerization.²³ In particular, a clear color darkening was perceived when directly adding this compound to liquid **Bz3** or preparing solid Bz-catalyst mixtures for the rest of monomers by evaporation of the corresponding acetone solutions (Fig. 2b).

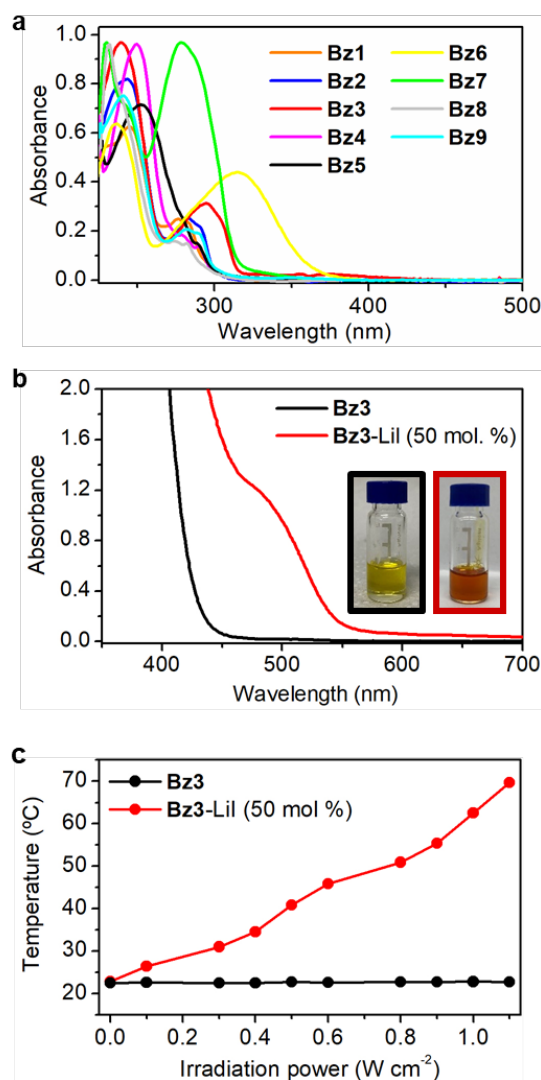


Fig. 2 a) UV-vis absorption spectra of all prepared (bis)benzoxazines in DCM ($c_{\text{Bz}} = 1.0 \times 10^{-5}$ M). b) UV-vis absorption spectra of pure benzoxazine **Bz3** and of its mixture with Lil (50 mol % relative to monomer content). Images of **Bz3** before (left) and after (right) the mixture are shown as insets. c) Temperature variation in liquid **Bz3** and **Bz3-Lil** (50 mol % relative to monomer content, 0.5 mL) under laser irradiation at $\lambda_{\text{exc}} = 532$ nm (spot diameter = 1 cm). Maximum temperature values reached after around 5 min of irradiation at each power.

To further investigate this behavior, Bz samples with high Lil amounts were prepared (50 mol % relative to monomer concentration) and analyzed by UV-vis absorption as neat liquids (**Bz3**) or concentrated acetone solutions (**Bz1**, **Bz2**, **Bz4-Bz9**). As shown in Fig. 2b and Figs. S1-S9 in the ESI[†], a clear red-shifting of the absorption spectrum into the visible range was observed in all the cases and, indeed, the emergence of a new defined visible absorption band could be identified for most samples ($\lambda_{\text{abs}} \sim 400 - 550 \text{ nm}$). Importantly, none of these spectral changes could be attributed to the intrinsic absorption properties of the catalyst, which is a white solid that only absorbs in the UV region (Fig. S10 in the ESI[†]). Instead, they should arise from its interaction with the Bz monomers. Based on our previous suggestion that metal ions such as Li^+ coordinate to the heteroatoms of the oxazine ring to favor Bz ring-opening polymerization,^{23,24} herein we hypothesize that the resulting complexes present bathochromically displaced absorption. Actually, a similar behavior has already been reported for aromatic chromophores bearing O- and N-coordinating groups upon complexation to lithium ions.⁶¹ To demonstrate such interaction in the case of Bz monomers, we investigated the coordination of Li^+ ions to **Bz3** by means of additional spectrophotometric experiments. This allowed us to determine a 1:1 stoichiometry and a low association constant ($K_a = 0.48 \text{ M}^{-1}$) for the **Bz3**-Lil complex, which is consistent with the high concentrations needed to observe absorption changes upon metal salt addition (Fig. S11a in the ESI[†]).

Because of the red-shifted absorption of Bz-Lil systems, they can be excited with visible light. No emission was subsequently detected for any of these samples, which suggests that their photoexcited species mainly decay via internal conversion – i.e., generating heat by converting electronic excitation into vibrational energy. This photothermal effect was proven by irradiating a neat solution of Lil in **Bz3** (50 mol % relative to monomer content) with increasing intensities of green laser light ($\lambda_{\text{exc}} = 532 \text{ nm}$) while monitoring temperature with an IR probe. After a short incubation time ($\sim 5 \text{ min}$), constant temperatures were reached above room temperature, whose actual values rose with the photoexcitation power (Fig. 2c). Surprisingly, a sudden change in color from orange to red was observed for the **Bz3**-Lil solution when photothermally heated with the highest power intensities assayed ($1.0 - 1.1 \text{ W cm}^{-2}$), which suggested us that monomer reactivity was taking place at the temperatures reached in this case. By contrast, neither color change nor temperature increase was observed when irradiating pure **Bz3** samples at the same conditions (Fig. 2c).

Photothermal polymerization of benzoxazines

Taking advantage of the photothermal behavior of benzoxazine-Lil systems, we attempted their photoinduced polymerization in liquid (**Bz3**) and solid powder samples (**Bz1**, **Bz2**, **Bz4-Bz9**). In a first step, we prepared Bz-Lil systems with a 15 mol % catalyst concentration relative to monomer content, which were irradiated with a pulsed laser at $\lambda_{\text{exc}} = 532 \text{ nm}$ and 1.1 W cm^{-2} for $t_{\text{irr}} = 100 \text{ min}$ at ambient conditions. As all the resulting samples were found to be soluble in organic solvents except for bisbenzoxazine **Bz9**, we could estimate the polymerization efficiency for **Bz1-Bz8** by ^1H NMR analysis. With

this goal, we focused our attention on the peaks arising from the methylene oxazine protons of the monomers, whose defined signals disappear upon polymerization and give rise to the formation of a variety of new resonances at $\delta \sim 3.5 - 6.0$ that are generally attributed to the large number of different structures formed upon polymerization^{23,24} (Fig. 3a). By comparing the integrals of these different sets of monomer and polymer signals, we could estimate the evolution of the polymerization process in time using a methodology previously reported by us²⁴ (see the ESI[†] for further details).

Interestingly, none of the benzoxazine monomers polymerized neither upon irradiation in the absence of the catalyst nor in the dark when mixed with Lil at room temperature. These results are consistent with (a) the negligible visible absorbance of pure **Bz1-Bz9**, and (b) the limited capacity of catalysts such as Lil to decrease their T_p , which still lie above 100°C even for the 15 mol % concentration tested (Table S3 and Figs. S12-S20 in the ESI[†]). By

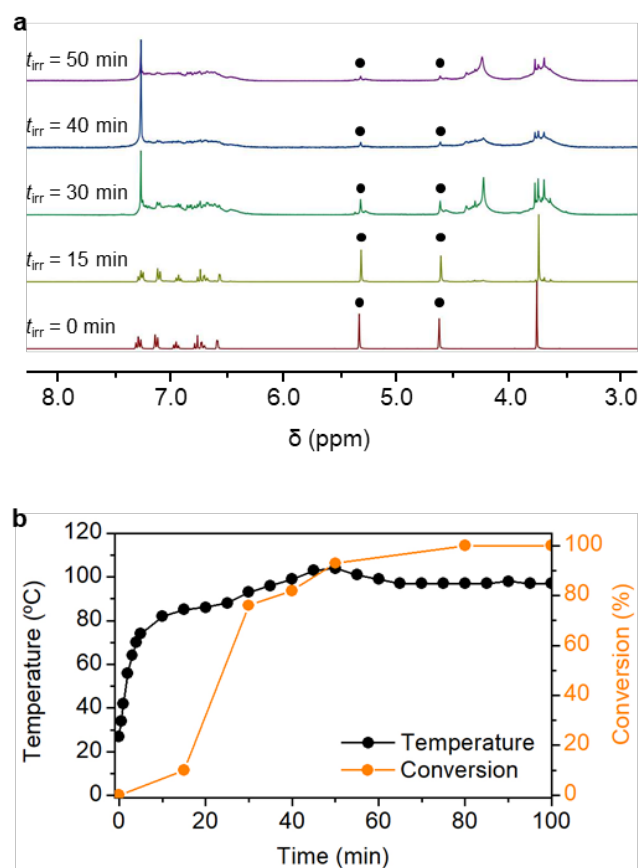


Fig. 3 a) Variation of the ^1H NMR spectrum (CDCl_3 , 360 MHz) of the **Bz3**-Lil system during photoirradiation at $t_{\text{irr}} = 0, 15, 30, 40$ and 50 min ($c_{\text{Lil}} = 15 \text{ mol \%}$ relative to monomer content; $\lambda_{\text{exc}} = 532 \text{ nm}$, power density = 1.1 W cm^{-2}). The black circles indicate the position of the signals of the methylene oxazine protons that disappear upon polymerization. The insets show photographs of **Bz3**-Lil before and after irradiation, which demonstrates the phototransformation of the initial liquid monomer into a solid polymer material. b) Evolution of the reaction mixture temperature and conversion during visible light irradiation of **Bz3**-Lil ($c_{\text{Lil}} = 15 \text{ mol \%}$ relative to monomer content; $\lambda_{\text{exc}} = 532 \text{ nm}$, power density = 1.1 W cm^{-2}).

contrast, illumination of Bz-Lil systems led to monomer polymerization for all monobenzoxazines **Bz1-Bz8** (Fig. S22 in the ESI†), which were converted from liquid or solid powders to homogeneous solid materials. Actually, full monomer conversion was observed in all the cases for irradiation times shorter than 100 min. For instance, quantitative polymerization at these conditions was observed for **Bz3** at $t_{\text{irr}} = 50$ (**Bz3-Lil**) and **Bz6** at $t_{\text{irr}} = 70$ min. In the case of **Bz9**, an insoluble solid was obtained in this way, a result that is in agreement with the capacity of this compound to lead to extensively cross-linked polymer networks.⁶⁰ Actually, when incubating the material obtained upon photoirradiation of **Bz9** with organic solvents and analyzing the resulting filtrates by ¹H NMR, no residual monomer signals could be identified, thus confirming quantitative conversion also for this monomer.

To investigate the mechanism for Bz photopolymerization at our experimental conditions, we simultaneously monitored the temperature changes and monomer conversion during the irradiation of **Bz3-Lil** with green laser light (Fig. 3b). A fast increase in temperature until $T \sim 80$ °C was registered for this sample after a few minutes ($t_{\text{irr}} < 10$ min), while negligible reactivity was observed. Consequently, photothermal effects imparted after visible light absorption must be responsible for such initial heating. Next, Bz polymerization was triggered and most of the monomer was consumed ($\sim 80\%$) without a significant rise in temperature ($T \sim 90$ °C), which only eventually increased up to $T \sim 100$ °C during the last stages of the reaction. Interestingly, these temperature values lie close to the lower limit of the polymerization temperatures determined for **Bz3** with 15 mol % content of Lil in the dark by DSC ($T_{\text{p, onset}} = 141.2$ °C, Table S3 in the ESI†) and, indeed, we observed that such a monomer-catalyst system polymerizes when externally heated at $T \sim 90$ °C for 1 h. Accordingly, our measurements support the photothermal nature of the light-induced reaction observed for **Bz3-Lil** – i.e., it is not only related with the absorption red-shift accomplished upon monomer-metal ion interaction, but also to the photothermal effects produced under illumination.

This conclusion was further corroborated by several additional experiments. First, no polymerization was observed when conducting the irradiation of monomer-catalyst samples at 0 °C in an ice bath. Second, by turning off the illumination source when reaching ca. 50% monomer conversion ($t_{\text{irr}} = 22.5$ min), the temperature of the sample rapidly decreased and the polymerization process stopped (Fig. S23 in the ESI†). Finally, when restricting the excitation to a small area of a bulk mixture, frontal polymerization – i.e., reactivity propagation outside of the illumination region – did not take place (Fig. S24 in the ESI†). Overall, these results unambiguously prove that light-induced polymerization at our experimental conditions proceeds at high temperatures, which we achieve locally by the photothermal effects imparted upon irradiation of visible-absorbing Bz-catalyst systems. As a result, our strategy enables efficient photopolymerization of benzoxazines, in contrast to previous reports where light was only employed for monomer initiation and did not induce photothermal heating.^{32,34}

To further explore the scope of our photothermal strategy towards PBz, we also investigated the effect of the substitution

pattern of the Bz monomer on the photopolymerization process. With this goal, we considered the case of **Bz10**, a monobenzoxazine bearing methyl substituents both in *ortho* and *para* positions (see section 2.4 in the ESI†). Upon addition of 15 mol % of Lil relative to monomer content and irradiation of the resulting powder mixture at $\lambda_{\text{exc}} = 532$ nm and 1.1 W cm^{-2} , less efficient photopolymerization was observed for **Bz10** relative to *p*-substituted benzoxazines **Bz1-Bz9**. Thus, only 58% monomer conversion was determined after $t_{\text{irr}} = 100$ min for **Bz10**, which could not be fully polymerized even after $t_{\text{irr}} = 300$ min (89% conversion). This result is consistent with the lower reactivity reported for *o,p*-disubstituted benzoxazines due to the blocking of the preferred sites for polymerization – i.e., the sites *ortho* and *para* to the phenolic position –, which typically react at higher temperatures through the arylamine group.⁶² Actually, this was proven by DSC measurements in our case, as we determined a $T_{\text{p, onset}} = 271.2$ °C for the pure *o,p*-dimethylsubstituted **Bz10** that is about 10 °C higher than for the pure *p*-methylsubstituted **Bz2** (Table S3 and Fig. S21 in the ESI†). Interestingly, these results are in agreement with the conclusions from our mechanistic investigation: the efficiency of our photopolymerization strategy depends on the capacity to generate sufficiently high photothermal heat upon irradiation as to reach the temperatures needed for the onset of thermal polymerization for each given monomer-catalyst system, a temperature threshold that can be largely affected by the Bz substitution pattern and the electronic nature of the substituents.

Optimization of the photothermal polymerization of benzoxazines

Once demonstrated the capacity to extensively photopolymerize Bz-Lil systems without the need of external heating, we pursued the optimization of the reaction conditions. Most of these studies were conducted for **Bz3** because of its high visible absorption and reactivity when mixed with Lil as well as its liquid nature, which facilitates the preparation and manipulation of the monomer-catalyst samples.

To start with, we investigated the effect of other metal salts different from Lil on photoreactivity, which we selected from some of the catalysts previously evaluated in our group for the thermal polymerization of benzoxazines:²⁴ Zn(OTf)₂, LiClO₄ and FeCl₃ (Fig. S10 in the ESI†). Although all of them promoted visible light-induced polymerization when mixed with **Bz3**, the best results were obtained with Zn(OTf)₂ (Table 1). Thus, **Bz3-Zn(OTf)₂** samples could be fully photopolymerized in just 6 min, which is about 10-fold faster than for **Bz3-Lil** under equivalent irradiation conditions. In addition, a similar optimal behavior was preserved when attempting the photopolymerization of other monobenzoxazines such as **Bz1**, **Bz2** and **Bz4** and bisbenzoxazine **Bz9** with Zn(OTf)₂ (Table 1). We ascribe this situation to two main factors. First, the larger absorption measured for Bz-Zn(OTf)₂ in the visible region relative to Bz-Lil even at lower metal salt concentrations (Figs. S1-S4 and S9 in the ESI†), probably due to the higher coordination capacity of Zn²⁺ ions.⁶³ As a result, irradiation of Bz-Zn(OTf)₂ must lead to much stronger photothermal effects. Second, the larger capacity of Zn(OTf)₂ to reduce the T_{p} of Bz in the dark ($T_{\text{p, onset}} = 56.4$ °C for **Bz3**), as proven by DSC (Table S3 in the ESI†). Consequently,

Table 1 Optimization of photopolymerization conditions for Bz-catalyst systems^a

Monomer	Catalyst	c_{catalyst}^b (mol %)	Irradiation		Conversion (%)
			Power (W cm ⁻²)	Time (min)	
Bz3	Zn(OTf) ₂	15	1.1	10	100 ^c
	LiClO ₄	15	1.1	100	68
	FeCl ₃	15	1.1	10	100
	ZnI ₂	15	1.1	10	77
Bz1	Zn(OTf) ₂	15	1.1	10	100 ^c
Bz2	Zn(OTf) ₂	15	1.1	10	100 ^c
Bz4	Zn(OTf) ₂	15	1.1	10	100
Bz9	Zn(OTf) ₂	15	1.1	10	59 ^d
Bz3	Lil	10	1.1	50	89
	Lil	5	1.1	50	89
	Lil	1	1.1	50	20
	Zn(OTf) ₂	10	1.1	10	95
	Zn(OTf) ₂	5	1.1	10	63
	Zn(OTf) ₂	1	1.1	10	0
	Zn(OTf) ₂	1	1.1	10	0
Bz3	Lil	15	1.0	50	63
	Zn(OTf) ₂	15	1.0	10	100
	Zn(OTf) ₂	15	0.9	10	87
	Zn(OTf) ₂	15	0.6	10	65
	Zn(OTf) ₂	15	9.6 ^e	10	100

^a λ_{exc} = 532 nm, monomer conversion determined by ¹H NMR. ^b Catalyst concentration relative to monomer content. ^c Quantitative monomer conversion achieved at t_{irr} = 6 min. ^d A soluble polymer material was obtained for bisbenzoxazine **Bz9** in this case, probably due to incomplete polymerization. ^e Irradiation with a cw laser at λ_{exc} = 532 nm instead of a pulsed laser.

the photothermal effects generated in this case should be more effective in triggering benzoxazine polymerization.

However, in contrast to Bz-Lil, Bz-Zn(OTf)₂ systems were found not to be stable when stored for hours under ambient conditions, which we attributed to triflic acid formation upon moisture absorption. For this reason, we also explored the use of ZnI₂ as a metal salt for Bz photothermal polymerization (Table 1). Although more stable samples were obtained with this catalyst, the change of the salt counteranion detrimentally affected the polymerization kinetics – e.g., only 77 % monomer conversion was achieved for **Bz3**-ZnI₂ at the same conditions that led to complete photopolymerization for **Bz3**-Zn(OTf)₂ (λ_{exc} = 532 nm, 1.1 W cm⁻², t_{irr} = 10 min). Such effect of the salt counteranion has already been described for the catalyzed thermal polymerization of benzoxazines, for which better results were obtained with Zn(OTf)₂ than ZnCl₂.²⁴ Therefore, the presence of triflate counteranions also seems to enhance the efficiency of our photothermal polymerization method, which could be ascribed to their better

leaving group character and/or their capacity to generate triflic acid that could aid to the initiation of Bz monomers.¹⁷

Next, we optimized the catalyst concentration and irradiation conditions required for efficient photothermal polymerization, for which we focused our attention on **Bz3**-Lil and **Bz3**-Zn(OTf)₂ samples (Table 1). In the case of Lil, we could decrease its concentration down to 5 mol % without drastically altering the polymerization time of **Bz3**-Lil samples. By contrast, slight decrements in irradiation power significantly slowed down the reactivity of these systems. A somewhat opposite situation was instead encountered for Zn(OTf)₂: while catalyst concentration could only be decreased to 10 mol % in order to preserve the polymerization kinetics, very fast monomer conversions were still observed for notably lower illumination power – e.g., 87 % **Bz3** polymerization could be achieved in only t_{irr} = 10 min despite decreasing the excitation intensity to 0.9 W cm⁻². Finally, we also explored the use of cw illumination instead of pulsed irradiation for **Bz3**-Zn(OTf)₂. Efficient photothermally-induced polymerization was also observed in this case, though the average photoexcitation power had to be increased about 9-fold to preserve the very rapid reaction kinetics (Table 1).

Even after optimization, a rather large concentration of catalyst is needed for our photopolymerization process to be efficient (> 5 mol %), which would lie entrapped within the solid material formed. Importantly, we determined the complexation constant between the polymer obtained and the remaining metal ions to be very low (K_a = 8.0 M⁻¹ for Lil and polymerized **Bz3**; Fig. S11b in the ESI[†]), which suggests that their effect on the structure of polybenzoxazines must be minor. Actually, this agrees with our previous studies on the coordination of Zn²⁺ to model benzoxazine compounds, which were found to be only important for short benzoxazine dimers containing two nearby phenol groups or one phenol and one amino groups.⁶⁴ Instead, metal complexation becomes much weaker in the presence of strong hydrogen-bonds between phenol groups, which is typically the case in polybenzoxazines.⁶⁴ In light of this, we attempted the removal of the metal ions from our photopolymerized materials, for which we focused on the **Bz3**-Zn(OTf)₂ system. Upon dissolution in cold acetone where Zn(OTf)₂ is very poorly soluble, we observed a 85 % reduction in triflate counterions from the photoproduct polymer by ¹⁹F NMR. In addition, we found that the ¹H NMR of this sample did not significantly vary upon purification, which corroborates our hypothesis that the structure of the photogenerated polymers must not be critically affected by the presence of residual metal ions.

Thermal vs photothermal polymerization of benzoxazines

To assess the effect of our photopolymerization process on the properties of PBz, we compared the behavior of the solid materials obtained from the photothermal and thermal polymerization of several benzoxazine monomers (**Bz1**-**Bz4** and **Bz9**, Table 2).

First, we observed that the photothermally-produced polymers were considerably soluble in many of the organic polar solvents tested – e.g., acetone, DMSO, ethyl acetate and CHCl₃. As already discussed, the only exception to this behavior is bisbenzoxazine **Bz9**,

Table 2 Properties of PBz prepared via thermal and photothermal polymerization^a

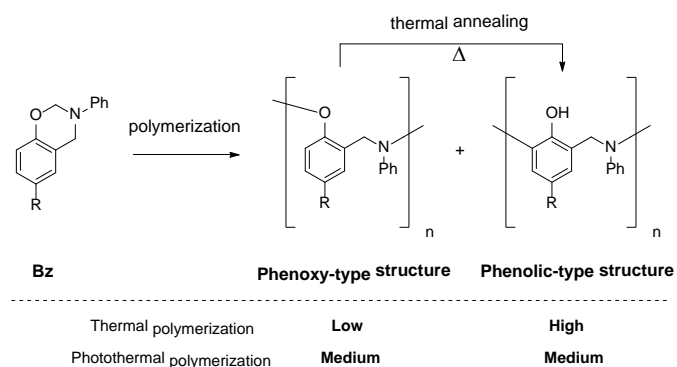
Monomer	Reaction	Catalyst ^b	Structure ^c (%)		T _g (°C)	Char yield ^d (%)
			Phenoxy	Phenolic		
Bz1	Thermal	-	Not soluble ^e		98.4	42
	Thermal	Lil	Not soluble ^e		93.7	38
	Thermal	Zn(OTf) ₂	0 ^e	100 ^f	102.2	41
	Photothermal	Lil	69	31	50.1	36
	Photothermal	Zn(OTf) ₂	74	26	53.3	44
Bz2	Thermal	-	Not soluble ^e		160.3	40
	Thermal	Lil	5 ^e	95 ^f	100.7	29
	Thermal	Zn(OTf) ₂	15	85	60.7	34
	Photothermal	Lil	56	44	56.0	37
	Photothermal	Zn(OTf) ₂	47	53	56.2	53
Bz3	Thermal	-	25	75	57.7	32
	Thermal	Lil	0	100	88.5	43
	Thermal	Zn(OTf) ₂	0	100	52.2	30
	Photothermal	Lil	50	50	53.4	48
	Photothermal	Zn(OTf) ₂	65	35	17.2	48
Bz4	Thermal	-	0 ^e	100 ^f	152.9	56
	Thermal	Lil	Not soluble ^e		- ^g	53
	Thermal	Zn(OTf) ₂	Not soluble ^e		- ^g	56
	Photothermal	Lil	45	55	60.6	53
	Photothermal	Zn(OTf) ₂	55	45	58.6	60
Bz9	Thermal	-	Not soluble ^e		166.3	34
	Thermal	Lil	Not soluble ^e		- ^g	29
	Thermal	Zn(OTf) ₂	Not soluble ^e		- ^g	16
	Photothermal	Lil	Not soluble ^e		61.1	33
	Photothermal	Zn(OTf) ₂	80 ^h	20 ^h	27.7	38

^a Thermal polymerizations were performed by heating at 180 °C, while photopolymerizations were conducted under pulsed laser excitation at $\lambda_{\text{exc}} = 532$ nm, power density = 1.1 W cm⁻², $t_{\text{irr}} = 100$ (Bz-Lil) or 10 min (Bz-Zn(OTf)₂) and ambient conditions. ^b $C_{\text{catalyst}} = 15$ mol % relative to monomer concentration. ^c Determined by ¹H NMR. ^d Measured after heating up to 800 °C. ^e Polymer not soluble in organic solvents. ^f Polymer sparingly soluble in DMSO and insoluble in the rest of organic solvents tested. ^g T_g values could not be determined. ^h Structure type ratio estimated for the polymerized fraction of the monomer.

which seems to form insoluble cross-linked materials when subjected to long irradiation times – e.g., for $t_{\text{irr}} = 100$ min with Lil. By contrast, thermal polymerization led to insoluble or sparingly soluble PBz not only for **Bz9**, but also for several of the monobenzoxazines tested depending on the catalyst used (Table 2). To investigate this issue in depth, we determined the gel content of the photothermal and thermal polymers obtained for **Bz3** and **Bz9**,

the two monomers exhibiting the largest variation in solubility upon polymerization (see the ESI† for further details). For **Bz3**, almost no difference in gel content was observed for the polymers obtained photothermally and thermally using Lil as a catalyst: 1 % and 0 %, respectively, which indicates that essentially only highly soluble linear polymer chains are obtained irrespective of the polymerization method. On the other hand, very large gel contents were measured for **Bz9** both upon photothermal and thermal polymerization with Lil (97 % and 98 %, respectively), which proves the formation of highly cross-linked insoluble networks in the two cases.

Despite the negligible effect of chemical cross-linking in the polymer materials formed from **Bz3** and, probably, the rest of *p*-substituted monobenzoxazines tested, it must be noted that their solubility can be strikingly affected by another structural feature: the distinct types of polymerized structures that can be obtained from benzoxazine monomers. These are the phenolic-type structure generated by electrophilic aromatic substitution after oxazine ring-opening and the phenoxy-type structure generated by nucleophilic substitution, which rearranges to the more stable phenolic structure upon heating (Scheme 3).^{6,7} Because of the strong intramolecular hydrogen bonding network that the phenolic-type polymer chains can form, a higher phenolic-to-phenoxy ratio must then result in lower solubility.^{6,7} To corroborate this hypothesis, we estimated the contribution of phenolic and phenoxy groups to the structure of the polymeric materials prepared, for which we applied a ¹H NMR analysis methodology previously established by us (Table 2, see the ESI† and Fig. S25-S28 for further details).²⁴ As already described, PBz obtained through thermal polymerization at high temperatures – e.g., at T = 180 °C – were mainly composed of phenolic-type polymer chains (> 75%), thus explaining their low solubilities. On the other hand, photothermally-produced PBz presented a much larger percentage of phenoxy-type structures (> 45%), thus justifying their higher solubilities. Most probably, the larger phenoxy-type content observed upon photopolymerization is due to the lower temperatures achieved during the process, which do not enable thermal rearrangement to the more stable phenolic forms. This would explain why similar phenoxy-to-phenolic ratios were obtained for all the monomers and catalysts by means of our photothermal approach, as comparable temperatures must be accomplished in all the cases upon irradiation.

**Scheme 3** Influence of the polymerization method on the phenolic-to-phenoxy structure ratio of PBz.

The phenoxy-to-phenolic ratio of PBz structure also affects their thermal and mechanical performances.^{6,7} We investigated this issue by determining the glass transition temperature (T_g) of the polymers obtained by DSC measurements (Figs. S29-S33 in the ESI[†]). As shown in Table 2, photothermally prepared polybenzoxazines mainly exhibited $T_g \sim 50$ -60 °C, whereas thermal polymerization conducted to much higher T_g values in most of the cases. These results are therefore consistent with the lower phenolic content of the photoproduced polymers and clearly demonstrate that different PBz materials are obtained when applying our photothermal method relative to conventional thermal polymerization. However, we found that, by thermally annealing the photopolymerized PBz at 150 °C for 2 h, nearly quantitative phenoxy-to-phenolic structure transformation occurred (Figs. S25-S28 in the ESI[†]), thus making these materials more similar to those directly obtained by thermal polymerization.

To further investigate this behavior, we analyzed in detail the effect caused by thermal annealing on the properties of the photoproduced polymers obtained from **Bz3** using $\text{Zn}(\text{OTf})_2$ as a catalyst. From a structural point of view, no increase in chemical cross-linking was observed, as the gel content (2 %) remained as low as for the purely photothermally and thermally polymerized materials. However, a clear change in phenoxy-to-phenolic ratio was measured (0:100), which matches the value determined upon thermal polymerization with the same catalyst. In addition, the thermal treatment of the photoproduced polymer led to an increment in T_g (from 17.2 °C to 63.2 °C), which makes it closer to the value registered for the thermally-polymerized material ($T_g = 52.2$ °C). Finally, we could prove that thermal annealing also largely enhances the mechanical properties of the photopolymerized materials. Thus, while we could not conduct dynamic mechanical analysis (DMA) of the photothermally-produced polymer of **Bz3** because of its high brittleness, its mechanical properties could be determined after thermal treatment. In particular, the following storage moduli were registered for the thermally-annealed material by DMA: 1855 MPa and 759.4 MPa at 0 °C and 20 °C, respectively, which are very resemblant to those obtained for the analogous PBz directly polymerized thermally (1678 MPa and 702.6 MPa at 0 °C and 20 °C, respectively). Consequently, all these results imply that our photopolymerization strategy can be employed to produce low- T_g benzoxazine materials – i.e., easier moldable polymers – with the inherent advantages of light-induced processes – i.e., spatial and time control –, which can be later toughened by thermal annealing to obtain polymers that reproduce the thermal and mechanical performance of conventional PBz.

By contrast, char yield, one of the relevant features of PBz, did not seem to be affected by the polymerization method – i.e., by their phenolic-to-phenoxy ratio. Thus, similar char yield values (at 800 °C) were registered by TGA experiments for the thermally- and photothermally-produced materials and, in some cases, they could be even higher for the photopolymerized benzoxazines (Table 2, Figs. S34-S38 in the ESI[†]). In addition, thermogravimetric measurements also uncovered that the thermal stability of the resulting PBz does not significantly vary with the polymerization

strategy, as temperatures higher than 300 °C were needed to observe large mass losses in all the cases (> 30%, Figs. S34-S38 and Table S4 in the ESI[†]).

Photolithography of benzoxazines

Irrespective of the physico-chemical properties of the resulting polymers, the main difference of our photopolymerization strategy relative to thermal PBz polymerization lies on the inherent advantages of light-induced reactions: they can be performed with extreme time (down to fs) and spatial (down to nm) control. As a result, this would open new avenues for the fabrication and processing of PBz materials through light-induced self-healing, photolithography or 3D printing, among other methods.

As a proof of concept, we applied our photothermal polymerization approach to undertake the preparation of PBz patterns by means of photolithography under ambient conditions (Fig. 4). For this, we prepared liquid **Bz3**- $\text{Zn}(\text{OTf})_2$ samples to which we added a small amount of bisbenzoxazine **Bz9** to favor chemical cross-linking of the resulting polymer matrices (9:1 **Bz3**:**Bz9** ratio). After deposition onto glass substrates, these formulations were illuminated with a computer-controlled photolithography instrument equipped with a focusable cw violet laser ($\lambda_{\text{exc}} = 405$ nm, Fig. S39 in the ESI[†]), thus generating defined solid features by local photothermal polymerization. Removal of the unreacted monomer-catalyst system by rinsing with organic solvents (e.g., ethyl acetate) finally allowed isolation of the complex target PBz patterns that could not be fabricated otherwise.



Fig. 4 Photopatterning of PBz by (a) casting a **Bz3**/**Bz9**- $\text{Zn}(\text{OTf})_2$ formulation onto glass (9:1 **Bz3**:**Bz9** ratio, $c_{\text{catalyst}} = 15$ mol % relative to the total monomer content), (b) irradiating this sample locally with a scannable cw violet laser ($\lambda_{\text{exc}} = 405$ nm, 33 W cm^{-2} , 10 mm s^{-1}) and (c) removing the excess of unreacted monomer.

Conclusions

In this work we report a novel photopolymerization strategy for polybenzoxazines, a class of technologically-relevant thermosets that require high temperatures for their synthesis and processing even when initiators or catalysts are employed. By mixing benzoxazine monomers with common metal salts typically used as polymerization catalysts, we observed the formation of complexes that exhibit visible light absorption and generate strong photothermal heating upon photoexcitation. As a result, irradiation of benzoxazine-catalyst samples with visible light under ambient conditions triggers extensive photothermal polymerization, a process that can be expanded to a large variety of mono- and bifunctional monomers and be completed in very short time scales. This is a remarkable improvement relative to previous photopolymerization methods proposed for benzoxazines, which

can only render incomplete monomer conversion. Although the polymer materials photoproducted herein are more soluble and show lower T_g values than when thermally polymerized, they preserve some of the main features of polybenzoxazines – e.g., high char yields. In addition, they can be toughened by subsequent thermal treatment, eventually exhibiting thermo-mechanical properties that are very similar to those of conventional polybenzoxazines. More importantly, our photothermal strategy allows the polymerization of benzoxazines with spatiotemporal control, a feature that we have exploited to generate lithographical polybenzoxazine patterns. Therefore, our work paves the way to the fabrication and processing of polybenzoxazines at ambient conditions using unprecedented light-based technologies such as photolithography and 3D printing.

Author Contributions

Notes and references

- 1 T. Meyer and J. Keurentjes. *Handbook of polymer reaction engineering*. Wiley-VCH. 2005.
- 2 T. F. Scott, B. A. Kowalski, A. C. Sullivan, C. N. Bowman and R. R. McLeod, *Science*, **2009**, 324, 913–917.
- 3 I. Kherbouche, Y. Luo, N. Félidj and C. Mangeney, *Chem. Mater.*, **2020**, **32**, 5442.
- 4 M. Layani, X. Wang and S. Magdassi, *Adv. Mater.*, **2018**, **30**, 1706344.
- 5 L. Y. Zhou, J. Fu and Y. He, *Adv. Funct. Mat.*, **2020**, **30**, 2000187.
- 6 H. Ishida and T. Agag. *Handbook of benzoxazine resins*. Elsevier. 2011.
- 7 H. Ishida and P. Froimowicz. *Advanced and emerging polybenzoxazine science and technology*. Elsevier. 2017.
- 8 H. Ishida and H. Y. Low. *Macromolecules*, **1997**, **30**, 1099–1106.
- 9 H. Ishida and D. Allen. *J. Polym. Sci. Polym., Phys.*, **1996**, **34**, 1019–1030.
- 10 X. Liu and Y. Gu. *J. Appl. Polym. Sci.*, **2002**, **84**, 1107–1113.
- 11 C. F. Wang, Y. C. Su, S. W. Kuo, C. F. Huang, Y. C. Sheen and F. C. Chang. *Angew. Chem. Int. Ed.*, **2006**, **45**, 2248–2251.
- 12 H. D. Kim and H. Ishida. *J. Appl. Polym. Sci.*, **2001**, **79**, 1207–1219.
- 13 N. K. Sini and T. Endo, *Macromolecules* **2016**, **49**, 8466–8478.
- 14 S. B. Shen and H. Ishida. *Polym. Compos.*, **1996**, **17**, 710–719.
- 15 N. N. Ghosh, B. Kiskan and Y. Yagci, *Prog. Polym. Sci.*, **2007**, **32**, 1344–1391.
- 16 J. Liu and H. Ishida. *Macromolecules*, **2014**, **47**, 5682–5690.
- 17 B. Lochab, M. Monisha, N. Amarnath, P. Sharma, S. Mukherjee and H. Ishida, *Polymers*, **2021**, **13**, 1260.
- 18 J. Dunker and H. Ishida, *J. Polym. Sci. Part A Polym. Chem.*, **1999**, **37**, 1913–1921.
- 19 A. Sudo, H. Yamashita and T. Endo, *J. Polym. Sci. Part A Polym. Chem.*, **2011**, **49**, 3631–3636.
- 20 Y. X. Wang and H. Ishida. *Polymer*, **1999**, **40**, 4563–4570.
- 21 H. D. Kim and H. Ishida, *Macromolecules*, **2000**, **33**, 2839–2847.
- 22 A. Sudo, S. Hirayama and T. Endo, *J. Polym. Sci. Part A Polym. Chem.*, **2010**, **48**, 479–484.
- 23 C. Liu, D. Shen, R. M. Sebastián, J. Marquet and R. Schönfeld. *Macromolecules*, **2011**, **44**, 4616–4622.
- 24 C. Liu, D. Shen, R. M. Sebastián, J. Marquet and R. Schönfeld. *Polymer*, **2013**, **54**, 2873–2878.
- 25 W. Zhang, P. Froimowicz, C. R. Arza, S. Ohashi, Z. Xin and H. Ishida, *Macromolecules*, **2016**, **49**, 7129–7140.
- 26 K. Zhang, Y. Liu, M. Han and P. Froimowicz, *Green Chemistry*, **2020**, **22**, 1209–1219.
- 27 B. Hao, L. Han, Y. Liu and K. Zhang, *Polym. Chem.*, **2020**, **11**, 5800–5809.
- 28 W. Zhao, B. Hao, Y. Lu and K. Zhang, *Eur. Polym. J.*, **2022**, **166**, 111041.
- 29 M. Soto, M. Hiller, H. Oschkinat and K. Koschek, *Polymers*, **2016**, **8**, 278.
- 30 H. Schäfer, A. Arnebold, J. Stelten, J. Marquet, R.M. Sebastián, A. Hartwig and K. Koschek, *J. Polym. Sci. Part A Polym. Chem.*, **2016**, **54**, 1243–1251.
- 31 S. K. Loke, E. P. S. Devaraju, V. Srinivasadesikan and R. K. Kottalanka, *RSC Adv.*, **2020**, **10**, 36275–36286.
- 32 F. Kasapoglu, I. Cianga, Y. Yagci and T. Takeichi, *T. J. Polym. Sci. A Polym. Chem.*, **2003**, **41**, 3320–3328.
- 33 Z. Deliballi, B. Kiskan and Y. Yagci, *Polym. Chem.*, **2021**, **12**, 5781–5786.
- 34 J. Salabert, R. M. Sebastián and J. Marquet. *Macromolecules*, **2018**, **51**, 3672–3679.
- 35 C. Wang and D. Astruc, *Chem. Soc. Rev.*, **2014**, **43**, 7188–7216.
- 36 A. Gellé, T. Jin, L. de la Garza, G. D. Price, L. V. Besteiro and A. Moores, *Chem. Rev.*, **2020**, **120**, 986–1041.
- 37 J. M. Walker, L. Gou, S. Bhattacharyya, S. E. Lindahl and J. M. Zaleski, *Chem. Mater.*, **2011**, **23**, 5275–5281.
- 38 K. G. Stamplecoskie, C. Fasciani and J. C. Scaiano, *Langmuir*, **2012**, **28**, 10957–10961.
- 39 M. Fedoruk, M. Meixner, S. Carretero-Palacios, T. Lohmüller and J. Feldmann, *ACS Nano*, **2013**, **7**, 7648–7653.
- 40 R. J. Fortenbaugh and B. J. Lear, *Nanoscale*, **2017**, **9**, 8555–8559.
- 41 R. J. Fortenbaugh, S. A. Carrozzi and B. J. Lear, *Macromolecules*, **2019**, **52**, 3839–3844.
- 42 W. M. Gramlich, J. L. Holloway, R. Rai, and J. A. Burdick, *Nanotechnology*, **2013**, **25**, 014004.
- 43 H. Lee, S. Chung, M. G. Kim, L. P. Lee and J. Y. Lee, *Adv. Healthc. Mater.*, **2016**, **5**, 1638–1645.
- 44 R. C. Steinhardt, T. M. Steeves, B. M. Wallace, B. Moser, D. A. Fishman and A. P. Esser-Kahn, *ACS Appl. Mater. Interfaces*, **2017**, **9**, 39034–39039.
- 45 A. H. Bonardi, F. Bonardi, F. Morlet-Savary, C. Dietlin, G. Noirbent, T. M. Grant and J. Lalevée, *Macromolecules*, **2018**, **51**, 8808–8820.
- 46 A. H. Bonardi, F. Bonardi, F. Dumur, D. Gigmes, J. P. Fouassier and J. Lalevée, *Macromol. Rapid Commun.*, **2019**, **40**, 1900495.
- 47 A. H. Bonardi, F. Dumur, D. Gigmes, Y. Y. Xu and J. Lalevée, *ACS Omega*, **2020**, **5**, 3043–3046.

Conflicts of interest

There are no conflicts to declare.

Acknowledgements

The authors acknowledge the Agencia Estatal de Investigación (PID2019-106171RB-100/AEI/10.13039/501100011033) and Generalitat de Catalunya (2017 SGR00465) for financial support. K. R.-M. thanks the Universitat Autònoma de Barcelona for his PIF pre-doctoral fellowship. We also thank Dr. Silvia De la Flor for conducting DMA experiments on our PBz samples.

- 48 H. Lee, S. Kim, C. Ryu and J. Y. Lee, *ACS Biomater. Sci. Eng.*, 2020, **6**, 1931-1939.
- 49 A. Caron, F. Dumur and J. Lalevée, *J. Polym. Sci.*, 2020, **58**, 2134-2139.
- 50 A. H. Bonardi, F. Bonardi, G. Noirbent, F. Dumur, D. Gigmes, C. Dietlin and J. Lalevée, *J. Polym. Sci.*, 2020, **58**, 300-308.
- 51 Y. Liang, Y. Bai, A. Q. Xie, J. Mao, L. Zhu and S. Chen, *Solar RRL*, 2022, **6**, 2100917.
- 52 P. Hu, H. Xu, Y. Pan, X. Sang and R. Liu, *ChemPhysChem*, 2022, **23**, 202100670.
- 53 K. M. Haas and B. J. Lear, *Chem. Sci.*, 2015, **6**, 6462-6467.
- 54 E. N. van Burns and B. J. Lear, *J. Phys. Chem. C*, 2019, **123**, 14774-14780.
- 55 R. Andreu, J. A. Reina and J. C. Ronda, *J. Polym. Sci. A: Polym. Chem.*, 2008, **46**, 3353-3366.
- 56 J. Dunkers and H. Ishida, *Spectrochim. Acta A*, 1995, **51**, 855-867.
- 57 M. E. Kuehne and E. A. Konopka, *J. Med. Chem.*, 1962, **5**, 257-280.
- 58 H. M. Ma, Y. Liu, Y. X. Liu, J. J. Qiu and C. Liu, *RSC Adv.*, 2015, **5**, 102441-102447.
- 59 A. Martos, R. M. Sebastián and J. Marquet, *Eur. Polym. J.*, 2018, **108**, 20-27.
- 60 M. A. Espinosa, V. Cádiz and M. Galia, *J. Appl. Polym. Sci.*, 2003, **90**, 470-481.
- 61 E. Villemin and O. Raccurt, *Coord. Chem. Rev.*, 2021, **435**, 213801.
- 62 H. Ishida and D. P. Sanders, *Polymer*, 2001, **42**, 3115-3125.
- 63 S. Upadhyay, A. Singh, R. Sinha, S. Omer and K. Negi, *J. Mol. Struct.*, 2019, **1193**, 89-102.
- 64 D. Shen, C. Liu, R. M. Sebastián, J. Marquet and R. Schönfeld, *J. Appl. Polym. Sci. A Polym. Chem.*, 2016, **133**, 44099.

Electronic supplementary information for Photothermal polymerization of benzoxazines

Kevin Reyes-Mateo, Jordi Marquet, Jordi Hernando* and Rosa M. Sebastián*

Table of contents

1. Materials and methods	S2
2. Synthesis of Bz1-Bz10	S3
2.1. Synthesis of 1,3,5-triphenyltriazine, 3	S3
2.2. Synthesis of benzoxazines Bz1-Bz8	S3
2.3. Synthesis of benzoxazine Bz9	S6
2.4. Synthesis of benzoxazine B10	S6
3. Spectrophotometric characterization of Bz-catalyst systems	S8
3.1. UV-vis absorption spectra of Bz-catalyst systems	S8
3.1. Studies of metal ion coordination with Bz3 and PBz3	S13
4. Polymerization of Bz and Bz-catalyst systems	S14
4.1. Preparation of Bz-catalyst systems for thermal and photothermal polymerization	S14
4.2. Determination of monomer conversion	S14
4.3. Thermal polymerization	S14
4.4. Photothermal polymerization	S21
4.5. Chemical stability of Bz3-catalyst systems	S22
5. Analysis of polybenzoxazines	S23
5.1. Determination of the phenoxy-phenolic structure ratio	S23
5.2. Determination of T_g	S25
5.3. Determination of char yield and thermal decomposition	S28
5.4. Determination of gel content	S31
5.5. Purification of polymer-catalyst samples	S31
6. Photolithography experiments	S33
7. NMR spectra	S34
8. References	S40

1. Materials and methods

Materials. Reagents and solvents for the synthesis of **Bz1-Bz10** as well as the metal salts employed as polymerization catalysts were purchased and used without further purification. Thin layer chromatography (TLC) was performed using Merck aluminium backed plates of TLC silica gel 60 F254, and flash column chromatography was performed using silica gel (230-400 mesh).

Nuclear magnetic resonance (NMR). ^1H NMR spectra were recorded on Bruker DPX250 (250 MHz) and DPX360 (360 MHz) spectrometers in CDCl_3 , acetone- d_6 and DMSO- d_6 . The δ -scale was normalized relative to the residual solvent signal (CDCl_3 : 7.26 ppm, acetone- d_6 : 2.05 ppm and DMSO- d_6 : 2.49 ppm).

UV-vis absorption spectrometry. Liquid samples and solutions were measured with an Agilent 8453 UV-visible spectrophotometer using Hellma Analytics glass cuvettes (1-cm and 2-mm light path).

Laser irradiation for photothermal polymerization. Unless indicated otherwise, samples were irradiated with the second harmonic ($\lambda_{\text{exc}} = 532$ nm, rep rate = 10 Hz, pulse width = 6 ns) of a Nd:YAG pulsed laser (Brilliant, Quantel). The photopolymerization of **Bz3**-Zn(OTf) $_2$ was also attempted with a cw laser at the same wavelength.

Temperature sensing. Temperature monitorization during photoirradiation experiments was conducted using a Testo 735 thermocouple.

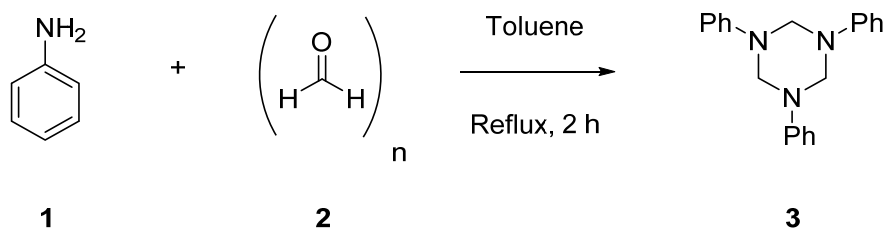
Differential scanning calorimetry (DSC). Samples were analyzed with a TA Instruments Q20 calorimeter using Tzero[™] pans and lids calibrated with indium ($T_m = 429.75$ K, $\Delta H_m = 3267$ kJ/mol). For all the samples, we used a heating rate of 10 °C/min and a N_2 flow of 50 mL/min.

Thermal gravimetric analysis (TGA). Samples were recorded with a TA Instruments TGA550 Discovery Series analyzed using a platinum HT crucible. For all the samples, we used a heating rate of 10 °C/min, a heating range of 30 – 800 °C, a N_2 flow of 40 mL/min and an air flow of 60 mL/min.

Dynamic mechanical analysis (DMA). Samples were tested in a TA Instruments DMAQ800 thermo-dynamo-mechanical analysis machine by using the three-point bending mode ($F = 1$ N/min). DMA experiments were performed on 32 x 12 x 3 mm rectangular polymer pieces prepared by either photothermal or thermal polymerization.

2. Synthesis of Bz1-Bz10

2.1. Synthesis of 1,3,5-triphenyltriazine, **3**¹

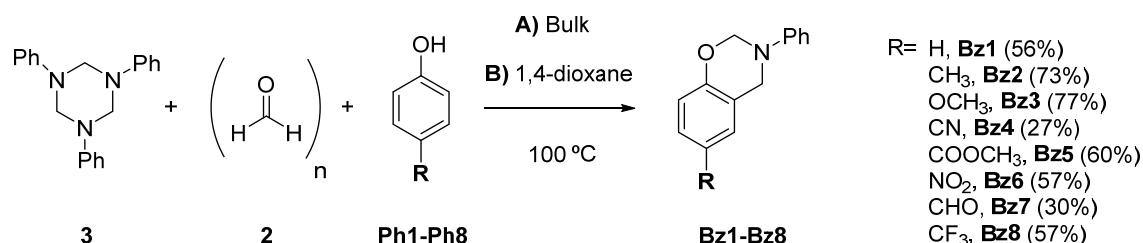


In a round-bottom flask equipped with a Dean-Stark apparatus, previously distilled aniline (**1**, 27.3 mL, 0.3 mol) and paraformaldehyde (**2**, 9.00 g, 0.3 mol) were added in 200 mL of toluene. The mixture was stirred under reflux for 2 h. The reaction crude was cooled down to room temperature, and the white precipitate formed was filtered and washed with *n*-hexane. The solid was dried under reduced pressure and triazine **3** was obtained as a crystalline white solid (19.60 g, 62.2 mmol, 62 %).

Spectroscopic data

¹H NMR (360 MHz, CDCl₃). δ: 7.21 (t, *J* = 8.0 Hz, 6H), 7.01 (d, *J* = 8.0 Hz, 6H), 6.86 (t, *J* = 7.3 Hz, 3H), 4.89 (s, 6H).

2.2. Synthesis of benzoxazines Bz1-Bz8



Method A: Bz1,¹ Bz2,² Bz3,¹ Bz4,³ Bz5⁴ and Bz7⁵

In a round-bottom flask, 1,3,5-triphenyltriazine (**3**, 1 eq.), paraformaldehyde (**2**, 1 eq.) and the respective phenol (**Ph1-Ph5** and **Ph7**, 1 eq.) were slowly stirred in bulk and heated up to 100 °C. Once the mixture was melted, stirring was increased during the reaction time (40 min – 2 h). Next, the reaction crude was cooled down to room temperature and dissolved in Et₂O (30 – 50 mL)^a. The resulted organic phase was washed with 2 M NaOH (3 x 30 – 50 mL) and distilled water (3 x 30 – 50 mL) and finally dried with anhydrous Na₂SO₄. After filtration, the solvent was

^a The addition of Et₂O must be done BEFORE the solution reaches room temperature, since a hard and insoluble solid is formed at this point.

evaporated under vacuum and the obtained benzoxazine was purified by flash column chromatography (silica gel). The exact conditions used for the synthesis and purification of **Bz1-Bz5** and **Bz7** are shown in Table S1.

Table S1. Experimental conditions for the synthesis of benzoxazines **Bz1-Bz5** and **Bz7**.

Bz	Amount of phenol	t_{reaction}	Flash column chromatography	Yield (%)	Appearance
Bz1 (R=H)	2.23 g (23.7 mmol)	2 h	Hexane/DCM (2:1)	56% (2.78 g)	Yellow solid
Bz2 (R=CH ₃)	1.30 g (12.0 mmol)	40 min	Hexane/DCM (3:1)	73% (1.97 g)	White solid
Bz3 (R=OCH ₃)	3.70 g (29.5 mmol)	2 h	Hexane/DCM (2:1)	77% (5.54 g)	Yellow liquid
Bz4 (R=CN)	1.43 g (12.0 mmol)	1 h	Hexane/DCM (7:3)	27% (0.77 g)	White solid
Bz5 (R=COOEt)	2.10 g (12.4 mmol)	2 h	No purification required	60% (2.10 g)	Yellow solid
Bz7 (R=CHO)	1.46 g (12.0 mmol)	1.5 h	Hexane/DCM (1:2)	30% (0.84 g)	Yellow solid

Spectroscopic data

Bz1: ¹H NMR (360 MHz, CDCl₃). δ (ppm): 7.29 (d, J = 8.1 Hz, 2H), 7.13 (m, 3H), 7.03 (d, J = 7.6 Hz, 1H), 6.95 (t, J = 7.0 Hz, 1H), 6.90 (t, J = 7.7 Hz, 1H), 6.83 (d, J = 8.2 Hz, 1H), 5.38 (s, 2H), 4.65 (s, 2H).

Bz2: ¹H NMR (360 MHz, CDCl₃). δ (ppm): 7.25 (m, 2H), 7.10 (d, J = 7.6 Hz, 2H), 6.92 (t, J = 7.5 Hz, 2H), 6.82 (s, 1H), 6.71 (d, J = 8.3 Hz, 1H), 5.34 (s, 2H), 4.60 (s, 2H), 2.25 (s, 3H).

Bz3: ¹H NMR (360 MHz, CDCl₃). δ (ppm): 7.29 (m, 2H), 7.12 (d, J = 8.0 Hz, 2H), 6.95 (t, J = 7.5 Hz, 1H), 6.77 (d, J = 8.8 Hz, 1H), 6.71 (dd, J = 8.8 Hz, J = 2.8 Hz, 1H), 6.58 (d, J = 2.8 Hz, 1H), 5.33 (s, 2H), 4.62 (s, 2H), 3.75 (s, 3H).

Bz4: ¹H NMR (360 MHz, CDCl₃). δ (ppm): 7.41 (dd, J = 8.5 Hz, J = 2.1 Hz, 1H), 7.30 (m, 3H), 7.10 (d, J = 8.1 Hz, 2H), 7.00 (t, J = 7.4 Hz, 1H), 6.87 (d, J = 8.5 Hz, 1H), 5.45 (s, 2H), 4.66 (s, 2H).

Bz5: ¹H NMR (250 MHz, CDCl₃). δ (ppm): 7.81 (dd, J = 8.7 Hz, J = 1.7 Hz, 1H), 7.76 (d, J = 2.1 Hz, 1H), 7.27 (t, J = 7.7 Hz, 2H), 7.10 (d, J = 7.6 Hz, 2H), 6.95 (t, J = 7.6 Hz, 1H), 6.82 (d, J = 8.7 Hz, 1H), 5.42 (s, 2H), 4.66 (s, 2H), 4.34 (q, J = 7.0 Hz, 2H), 1.37 (t, J = 6.8 Hz, 3H).

Bz7: ^1H NMR (250 MHz, CDCl_3). δ (ppm): 9.83 (s, 1H), 7.65 (d, $J = 7.6$ Hz, 1H), 7.59 (s, $J =$, 2H), 7.29 (d, $J = 7.6$ Hz, 1H), 7.11 (d, $J = 8.2$ Hz, 2H), 6.97 (t, $J = 7.0$ Hz, 1H), 6.91 (d, $J = 8.8$ Hz, 1H), 5.46 (s, 2H), 4.70 (s, 2H).

Method B: Bz61 and Bz84

In a round-bottom flask, 1,3,5-triphenyltriazine (**3**), paraformaldehyde (**2**, 1 eq.) and the respective phenol (**Ph6** and **Ph8**, 1 eq.) were mixed in 1,4-dioxane (15 mL). The solution was stirred for a given time at 100 °C. The reaction crude was cooled down to room temperature and the solvent was evaporated under vacuum. A yellow liquid was obtained and, after rinsing with Et_2O , the desired benzoxazine was achieved that was purified by flash column chromatography (silica gel). The exact conditions used for the synthesis and purification of **Bz6** and **Bz8** are shown in Table S2.

Table S2. Experimental conditions for the synthesis of benzoxazines **Bz6** and **Bz8**.

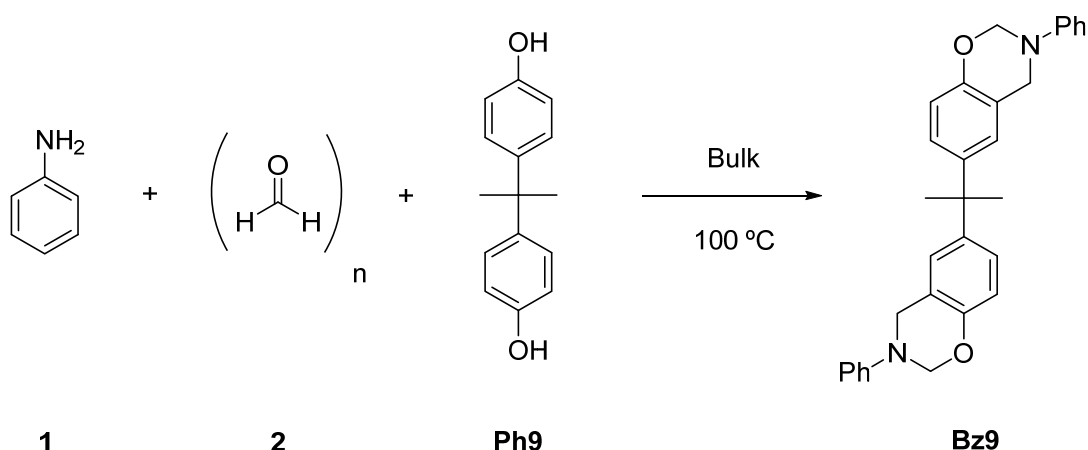
Bz	Amount of phenol	t_{reaction}	Flash column chromatography	Yield (%)	Appearance
Bz6 (R=NO ₂)	1.58 g (5.0 mmol)	18 h	Hexane/DCM (1:1)	57% (2.20 g)	Yellow solid
Bz8 (R=CF ₃)	2.3 g (8.2 mmol)	2 h	Hexane/DCM (1:1)	57% (1.31 g)	White solid

Spectroscopic data

Bz6: ^1H NMR (250 MHz, CDCl_3). δ (ppm): 8.06-7.96 (m, 2H), 7.28 (t, $J = 8.1$ Hz, 2H), 7.10 (d, $J = 7.5$ Hz, 2H), 6.99 (t, $J = 7.3$ Hz, 1H), 6.87 (d, $J = 8.1$ Hz, 1H), 5.47 (s, 2H), 4.70 (s, 2H).

Bz8: ^1H NMR (300 MHz, CDCl_3). δ (ppm): 7.51 (s, 1H), 7.44 (d, $J = 8.2$ Hz, 1H), 7.28 (d, $J = 7.8$ Hz, 1H), 7.24 (t, $J = 7.7$ Hz, 1H), 7.20 (d, $J = 8.0$ Hz, 2H), 7.18 (t, $J = 7.6$ Hz, 1H), 6.93 (m, 1H), 5.57 (s, 2H), 4.83 (s, 2H).

2.3. Synthesis of bisbenzoxazine Bz92

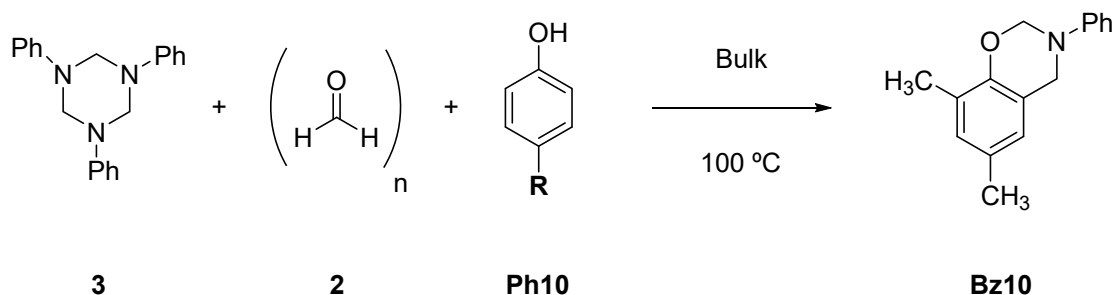


In a round-bottom flask, aniline (**1**, 1.8 mL, 20.0 mmol), paraformaldehyde (**2**, 1.20 g, 40.0 mmol) and bisphenol A (**4**, 2.30 g, 10.0 mmol) were mixed without solvent. The resulting solution was stirred for 45 min at 100 °C. The reaction crude was cooled down to room temperature and dissolved in Et₂O (\approx 40 mL).^b The resulting solution was dried in anhydrous Na₂SO₄ and filtered. The solvent was evaporated under vacuum and a yellowish solid foam was obtained.^c The resulting product was purified by flash column chromatography (silica gel, hexane/AcOEt (9:1)). Bisbenzoxazine **Bz9** was afforded in this way as a yellowish solid foam (2.50 g, 5.4 mmol, 54 %).

Spectroscopic data

¹H NMR (360 MHz, (CD₃)₂CO). δ (ppm): 7.23 (t, J = 8.0 Hz, 4H), 7.14 (dd, J = 9.0 Hz, J = 1.2 Hz, 4H), 7.00 (d, J = 2.2 Hz, 2H), 6.92 (dd, J = 8.7 Hz, J = 2.5 Hz, 2H), 6.86 (t, J = 7.2 Hz, 2H), 6.62 (d, J = 8.7 Hz, 2H), 5.40 (s, 4H), 4.63 (s, 4H), 1.56 (s, 6H).

2.4. Synthesis of benzoxazine Bz101



^b The addition of Et₂O must be done BEFORE the solution reaches to room temperature, since a hard and insoluble solid is formed at this point.

^c A 500 mL round-bottom flask is recommended to be used for these reagent quantities. When the solvent is evaporated under vacuum, a foam is formed that quickly expands. This is why a high volume is required as it is drying.

A mixture of phenol **Ph10** (1.83 g, 15 mmol), paraformaldehyde **2** (450 mg, 15 mmol), and 1,3,5-triphenylhexahydro-1,3,5-triazine **3** (1.575 g, 5 mmol) was stirred in air at 100 °C for 2 h. After cooled to room temperature, the mixture was dissolved in Et₂O and washed three times with 2 M NaOH and three times with water. The organic phase was dried with anhydrous Na₂SO₄, the diethyl ether was removed at low pressure and **Bz10** was obtained as a yellow oil without further purification (2.40 g, 10.1 mmol, 67%).

Spectroscopic data

¹H NMR (250 MHz, CDCl₃) δ (ppm): 7.25-7.31 (m, 2H, Ar-H, overlapping with the signal of CHCl₃), 7.12 (d, J = 7.5 Hz, 2H, Ar-H), 6.93 (t, J = 7.0 Hz, 1H, Ar-H), 6.81 (s, 1H, Ar-H), 6.69 (s, 1H, Ar-H), 5.37 (s, 2H, O-CH₂-N), 4.59 (s, 2H, Ar-CH₂-N), 2.23 (s, 3H, CH₃), 2.16 (s, 3H, CH₃).

3. Spectrophotometric characterization of Bz-catalyst systems

3.1. UV-vis absorption spectra of Bz-catalyst systems

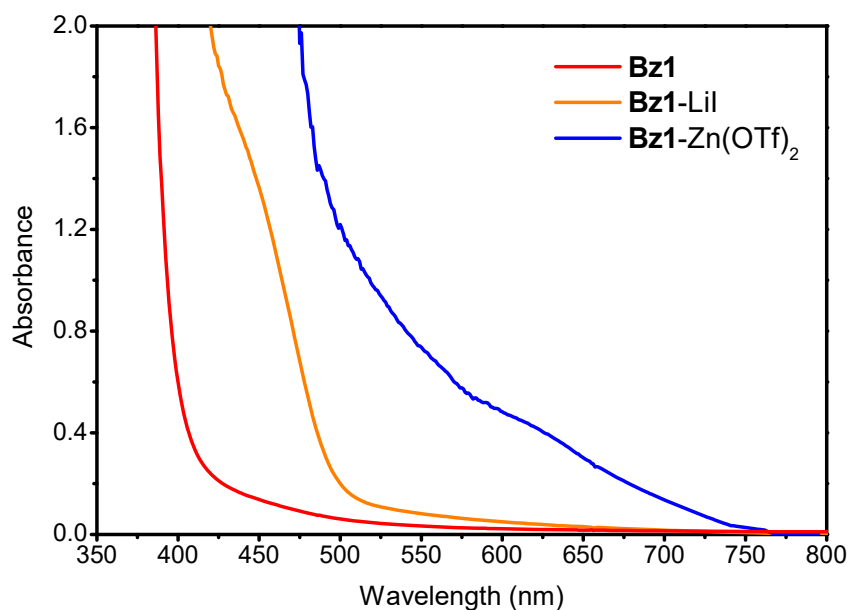


Fig. S1 UV-vis absorption spectra of **Bz1**, **Bz1-LiI** ($c_{\text{LiI}} = 50$ mol % relative to monomer content) and **Bz1-Zn(OTf)₂** ($c_{\text{Zn(OTf)}_2} = 15$ mol % relative to monomer content) in acetone ($c_{\text{Bz1}} = 3.9$ M). A 2 mm-thick glass cuvette was used.

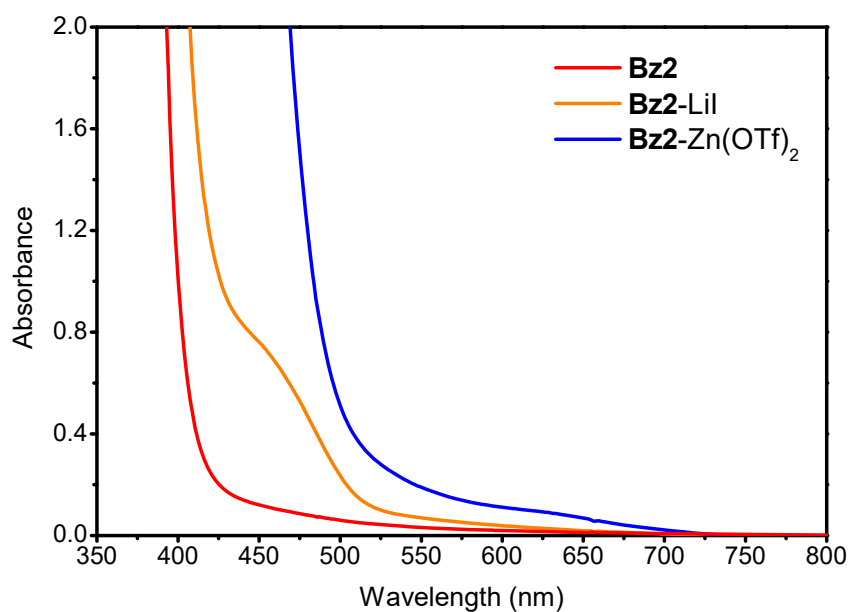


Fig. S2 UV-vis absorption spectra of **Bz2**, **Bz2-LiI** ($c_{\text{LiI}} = 50$ mol % relative to monomer content) and **Bz2-Zn(OTf)₂** ($c_{\text{Zn(OTf)}_2} = 15$ mol % relative to monomer content) in acetone ($c_{\text{Bz2}} = 3.9$ M). A 2 mm-thick glass cuvette was used.

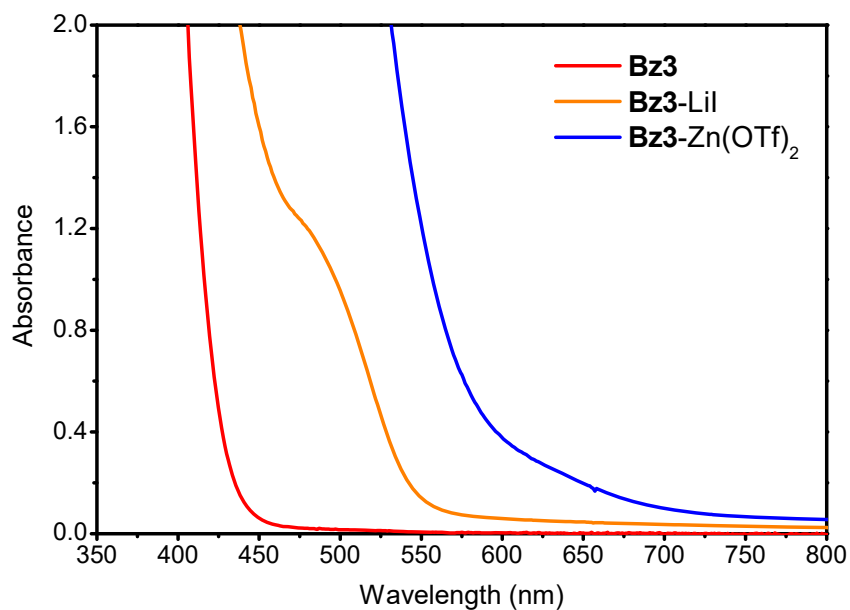


Fig. S3 UV-vis absorption spectra of **Bz3**, **Bz3-LiI** ($c_{\text{LiI}} = 50$ mol % relative to monomer content) and **Bz3-Zn(OTf)₂** ($c_{\text{Zn(OTf)}_2} = 15$ mol % relative to monomer content) in bulk liquid. A 2 mm-thick glass cuvette was used.

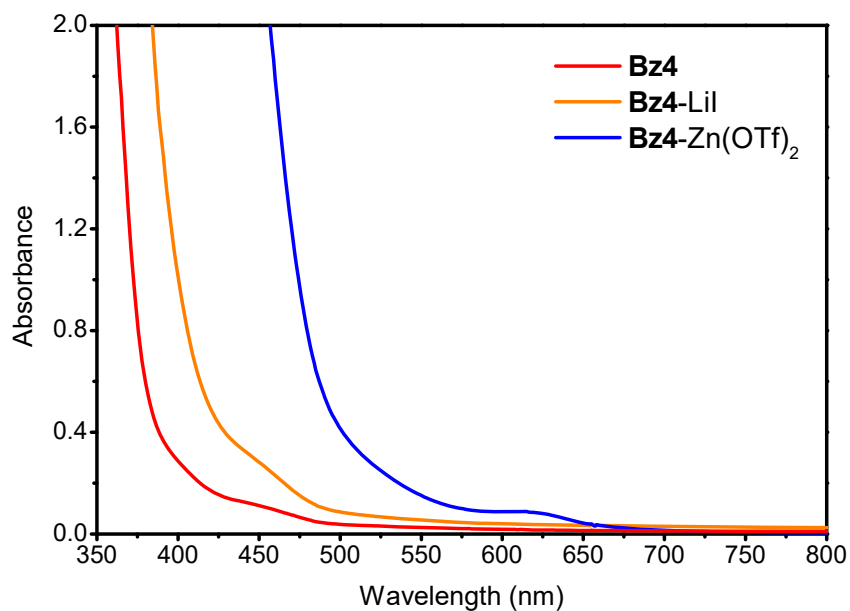


Fig. S4 UV-vis absorption spectra of **Bz4**, **Bz4-LiI** ($c_{\text{LiI}} = 50$ mol % relative to monomer content) and **Bz4-Zn(OTf)₂** ($c_{\text{Zn(OTf)}_2} = 15$ mol % relative to monomer content) in acetone ($c_{\text{Bz4}} = 1.2$ M). A 2 mm-thick glass cuvette was used.

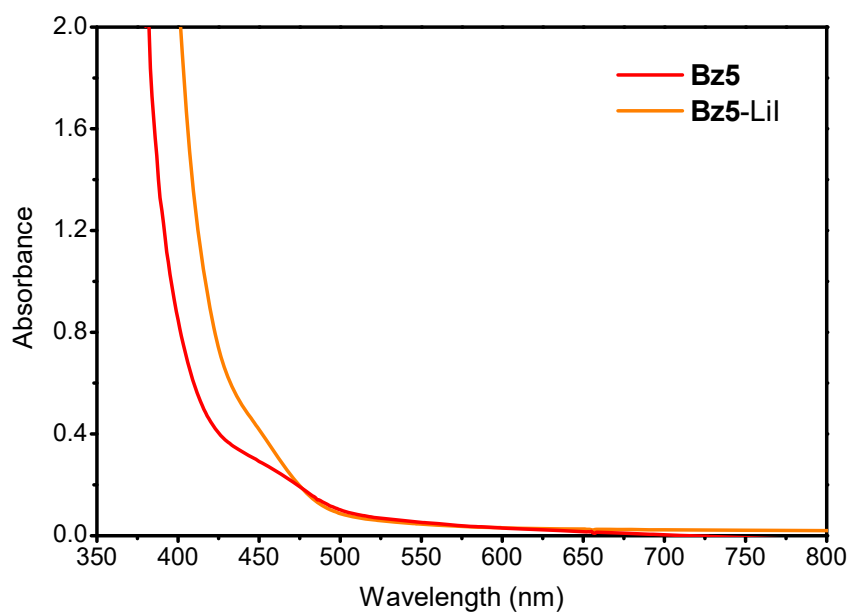


Fig. S5 UV-vis absorption spectra of **Bz5** and **Bz5-LiI** ($c_{\text{LiI}} = 50$ mol % relative to monomer content) in acetone ($c_{\text{Bz5}} = 2.4$ M). A 2 mm-thick glass cuvette was used.

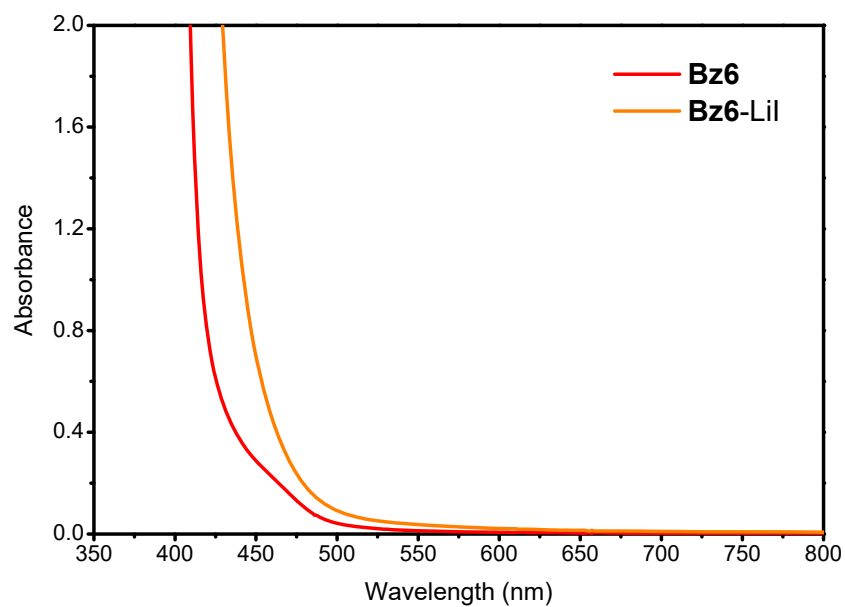


Fig. S6 UV-vis absorption spectra of **Bz6** and **Bz6-LiI** ($c_{\text{LiI}} = 50$ mol % relative to monomer content) in acetone ($c_{\text{Bz6}} = 1.0$ M). A 2 mm-thick glass cuvette was used.

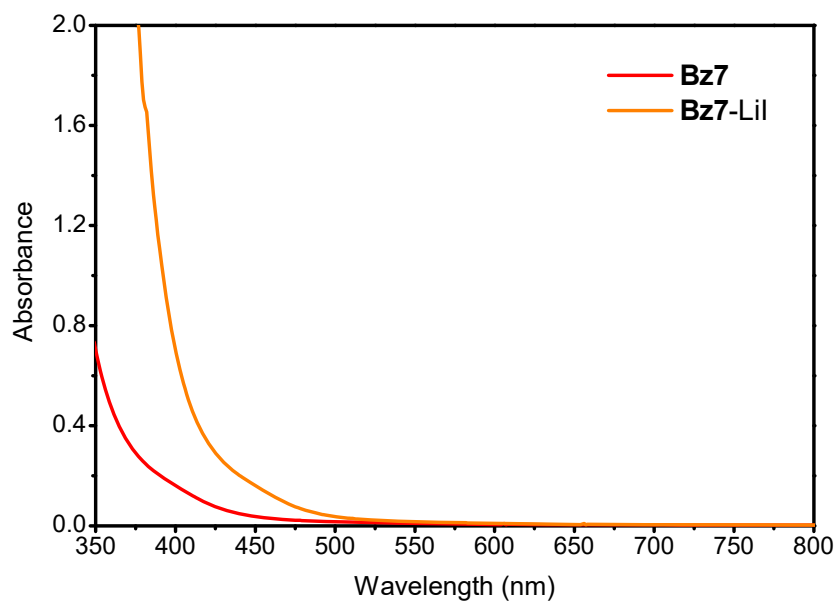


Fig. S7 UV-vis absorption spectra of **Bz7** and **Bz7-LiI** ($c_{\text{LiI}} = 50$ mol % relative to monomer content) in acetone ($c_{\text{Bz7}} = 2.0$ M). A 2 mm-thick glass cuvette was used.

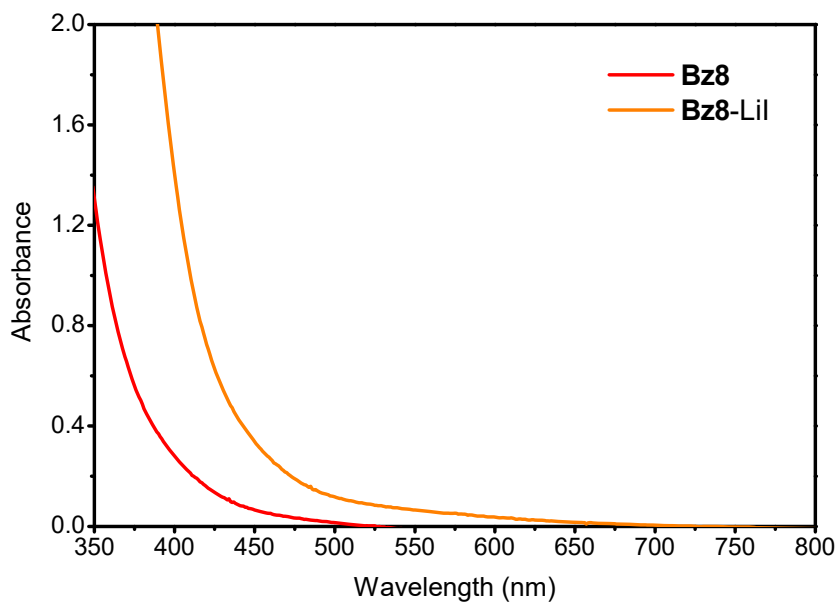


Fig. S8 UV-vis absorption spectra of **Bz8** and **Bz8-LiI** ($c_{\text{LiI}} = 50$ mol % relative to monomer content) in acetone ($c_{\text{Bz8}} = 1.9$ M). A 2 mm-thick glass cuvette was used.

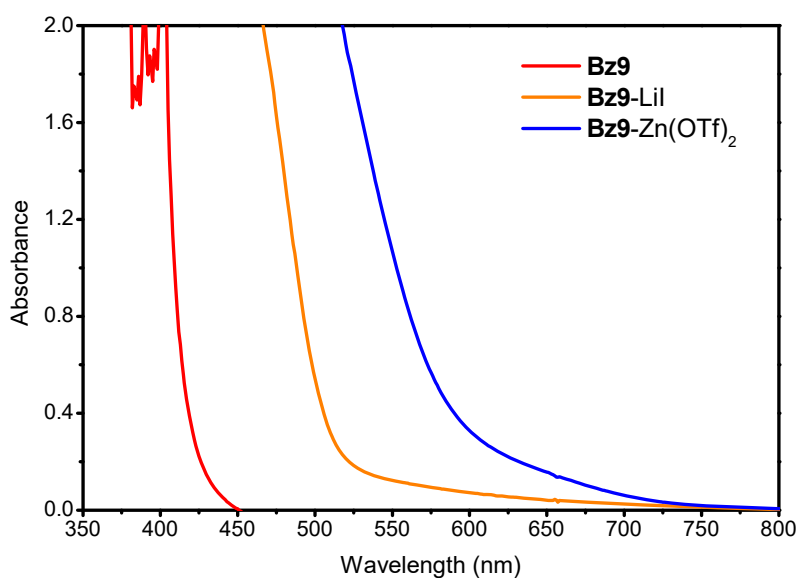


Fig. S9 UV-vis absorption spectra of **Bz9**, **Bz9-LiI** ($c_{\text{LiI}} = 50$ mol % relative to monomer content) and **Bz9-Zn(OTf)₂** ($c_{\text{Zn(OTf)}_2} = 15$ mol % relative to monomer content) in acetone ($c_{\text{Bz9}} = 2.4$ M). A 2 mm-thick glass cuvette was used.

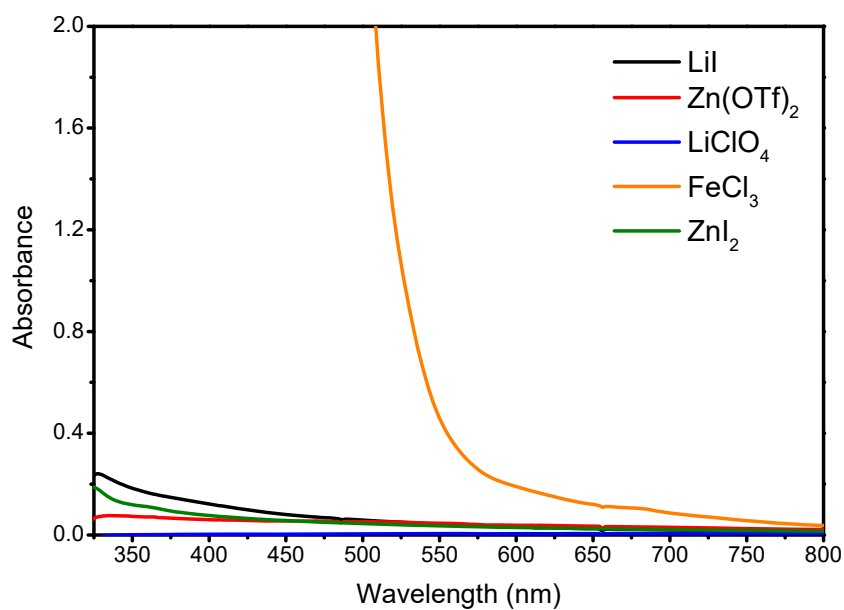


Fig. S10 UV-vis absorption spectra of LiI ($c_{\text{LiI}} = 1$ M), Zn(OTf)₂ ($c_{\text{Zn(OTf)}_2} = 0.3$ M), LiClO₄ ($c_{\text{LiClO}_4} = 0.3$ M), FeCl₃ ($c_{\text{FeCl}_3} = 0.3$ M) and ZnI₂ ($c_{\text{ZnI}_2} = 0.3$ M) in acetone.

3.2. Studies of metal ion coordination with Bz3 and PBz3

To determine the stoichiometries and association constants for the complexation between metal ions and benzoxazine monomers and polymers, we followed the same procedure previously used by us for similar systems.⁶ In particular, we used UV-vis spectrophotometry to monitor the spectral changes induced when: (a) adding increasing concentrations of Lil to neat liquid **Bz3** (Fig. S11a); (b) adding increasing concentrations of Lil to an acetone solution of a polybenzoxazine obtained by thermal polymerization of **Bz3** (Fig. S11b). The differences in absorbance measured in the visible region upon metal salt addition were then plotted against the metal salt concentration ($\lambda_{\text{abs}} = 480$ and 500 nm for Fig. S11a and S11b, respectively) and fitted to the Benesi–Hildebrand equation (1). In this equation, A is the absorbance upon metal salt addition, A_0 is the absorbance without metal salt, ε_c is the molar absorption coefficient of the complex, ε_0 is the molar absorption coefficient of the initial compound, $[N_0]$ is the concentration of the initial compound, K_a is the association constant, $[M]$ is the concentration of the metal salt for each addition, and n is the stoichiometric ratio.

$$\frac{1}{A - A_0} = \frac{1}{(\varepsilon_c - \varepsilon_0)[N_0]} + \frac{1}{(\varepsilon_c - \varepsilon_0)[N_0]K_a} \frac{1}{[M]^n} \quad (1)$$

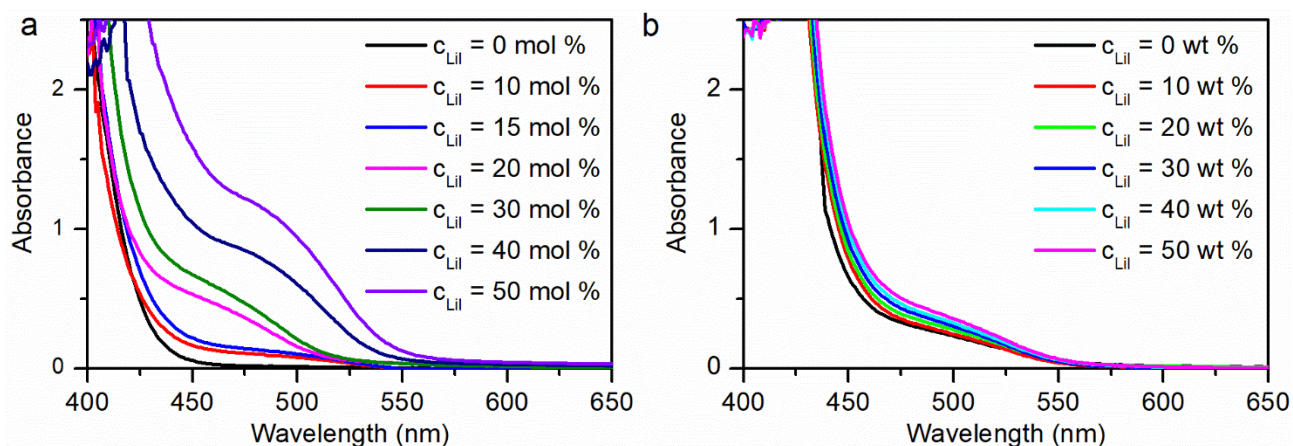


Fig. S11 (a) Variation of the UV-vis absorption spectrum of neat **Bz3** upon addition of increasing concentrations of Lil relative to monomer content. (b) Variation of the UV-vis absorption of thermally polymerized **PBz3** in acetone ($c_{\text{PBz3}} = 20 \text{ mg mL}^{-1}$) upon addition of increasing concentrations of Lil relative to polymer content.

4. Polymerization of Bz and Bz-catalyst systems

4.1. Preparation of Bz-catalyst systems for thermal and photothermal polymerization

Each given (bis)benzoxazine (0.2 – 0.3 g for **Bz1**, **Bz2** and **Bz4-Bz9**, 0.5 mL for **Bz3** and **Bz10**) was mixed with the catalyst of interest (typically, 15 mol % relative to monomer content) in a few milliliters of acetone.^d Once the mixture was completely solved, acetone was removed under reduced pressure and the corresponding benzoxazine-catalyst system was afforded.

4.2. Determination of monomer conversion

The conversion of all tested benzoxazine monomers during polymerization reactions was determined by ¹H NMR using previously reported equation 2.^{7,8} In this equation: (a) X is the integration of the ¹H NMR signals characteristic of the methylene units in the oxazine ring of the unreacted monomers ($\delta = 4.6$ and 5.4 ppm in CDCl₃); (b) Y is the sum of the integrals of the methylene signals of the unreacted monomers and the formed polymers ($\delta = 3.5 - 6.0$ ppm in CDCl₃) at a given polymerization time.

$$\text{Conversion (\%)} = \left[\frac{(Y - 2X)}{Y} \right] \cdot 100 \quad (2)$$

4.3. Thermal polymerization

Neat benzoxazine thermal polymerization: Each of the (bis)benzoxazines of interest was heated in a sand bath at 180 °C for 2 h.

Thermal polymerization of benzoxazine-catalyst systems: Each of the (bis)benzoxazine-catalyst samples prepared (see section 4.1) was heated in a sand bath at 180 °C for 2 h.

Determination of thermal polymerization temperature (T_p): DSC was used to determine the thermal polymerization temperature of neat Bz monomers and monomer-catalyst systems. Two main thermal transitions were identified in the thermograms of these samples: (a) an endothermic signal arising from the melting of the Bz monomer (except for liquid **Bz3**); (b) an exothermic peak assigned to the polymerization reaction. The onset and peak temperatures of the DSC polymerization signal determined for all the samples under study are given in Table S3, while the corresponding thermograms are shown in Figs. S12-S21.

^d Huge solvent volumes are not required for LiI, since its solubility in acetone is around 400 mg/mL. By contrast, Zn(OTf)₂ is barely soluble in acetone at room temperature. For this reason, the metal salt must be solved in hot acetone under vigorous stirring.

Table S3. Thermal polymerization temperature of neat Bz monomers and Bz-catalyst systems.

Bz	Catalyst	c_{catalyst} (mol %) ^a	T _{p, onset} (°C)	T _{p, peak} (°C)
Bz1	-	-	265.1	269.7
	LiI	15	184.7	194.0
	Zn(OTf) ₂	15	61.8	77.2
Bz2	-	-	263.9	273.6
	LiI	15	189.6	201.2
	Zn(OTf) ₂	15	77.2	87.0
Bz3	-	-	249.4	258.9
	LiI	15	141.2	159.4
	Zn(OTf) ₂	15	56.4	82.4
Bz4	-	-	220.9	225.0
	LiI	15	167.5	180.4
	Zn(OTf) ₂	15	93.5	99.6
Bz5	-	-	243.9	249.0
	LiI	15	171.1	188.9
Bz6	-	-	189.4	194.5
	LiI	15	153.9	167.2
Bz7	-	-	223.9	229.2
	LiI	15	138.1	159.5
Bz8	-	-	248.5	250.6
	LiI	15	181.2	190.6
Bz9	-	-	214.6	232.3
	LiI	15	160.2	182.8
Bz10	-	-	271.2	281.9
	LiI	15	177.8	199.5

^a Relative to monomer concentration.

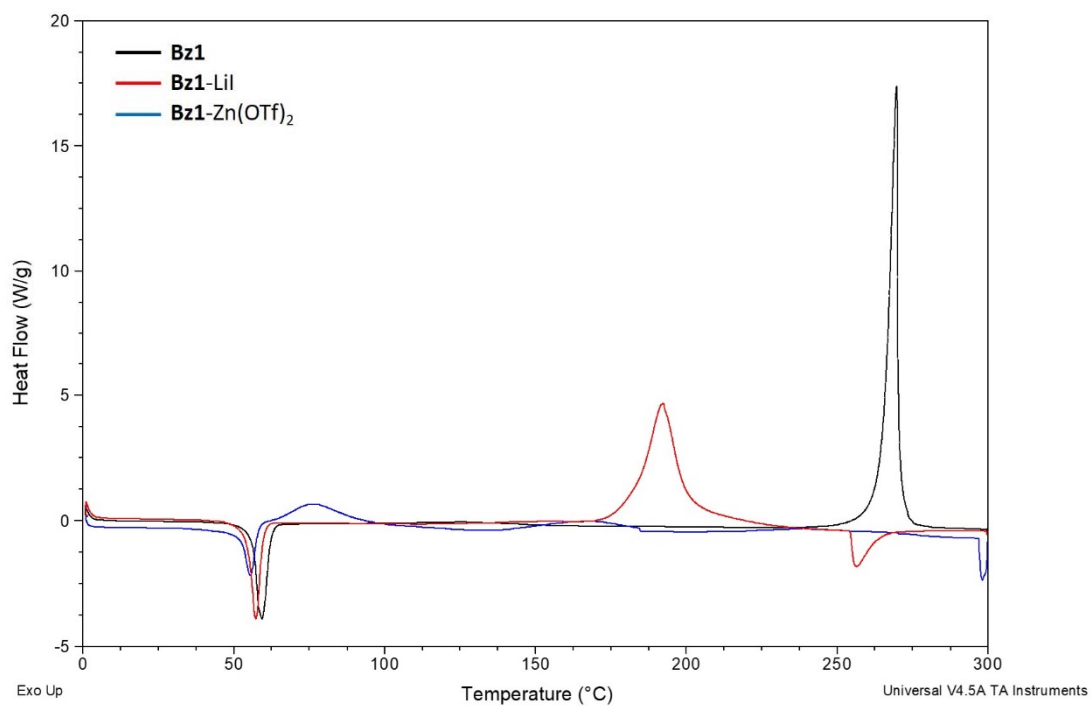


Fig. S12 DSC thermogram of neat **Bz1** and **Bz1**-catalyst systems.

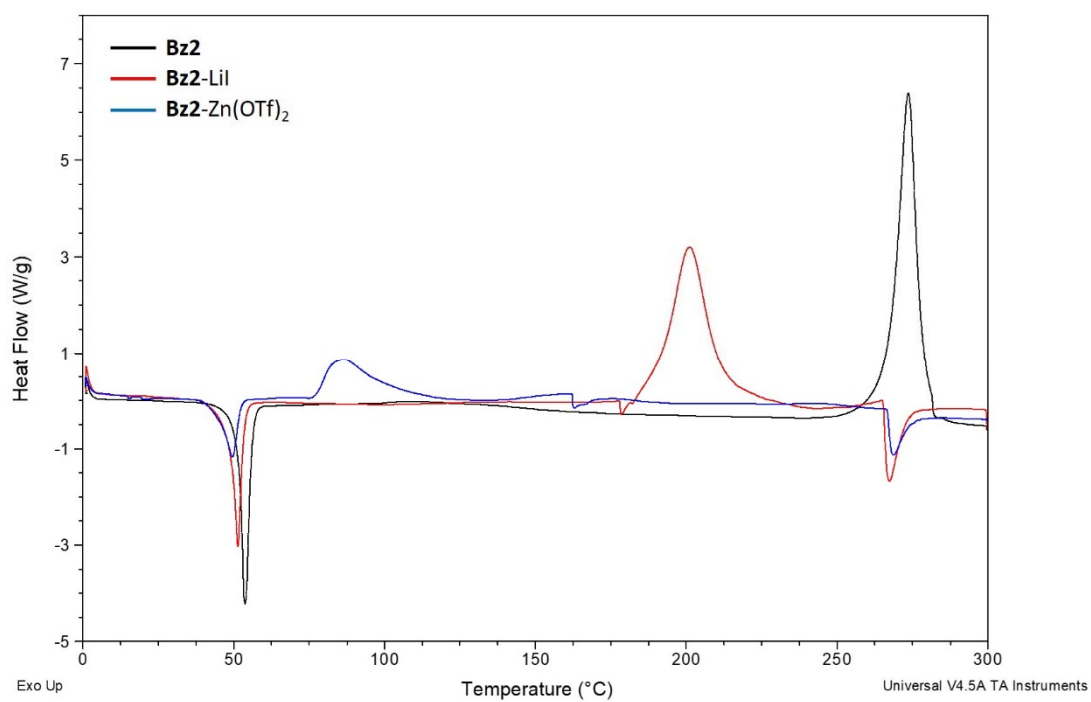


Fig. S13 DSC thermogram of neat **Bz2** and **Bz2**-catalyst systems.

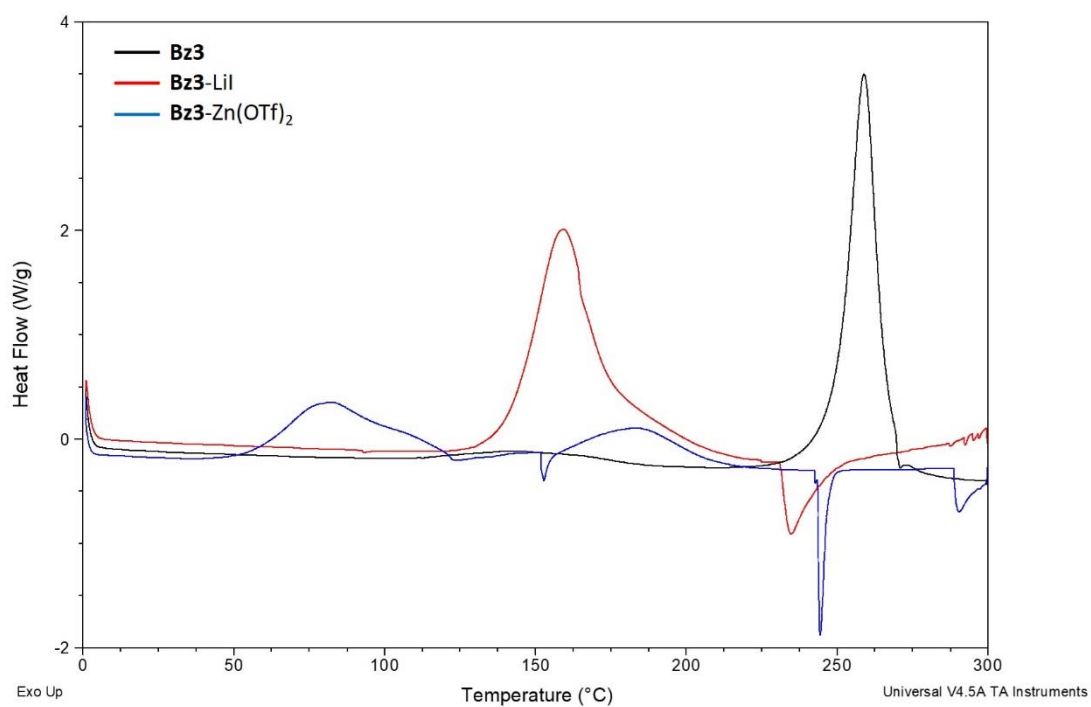


Fig. S14 DSC thermogram of neat **Bz3** and **Bz3**-catalyst systems.

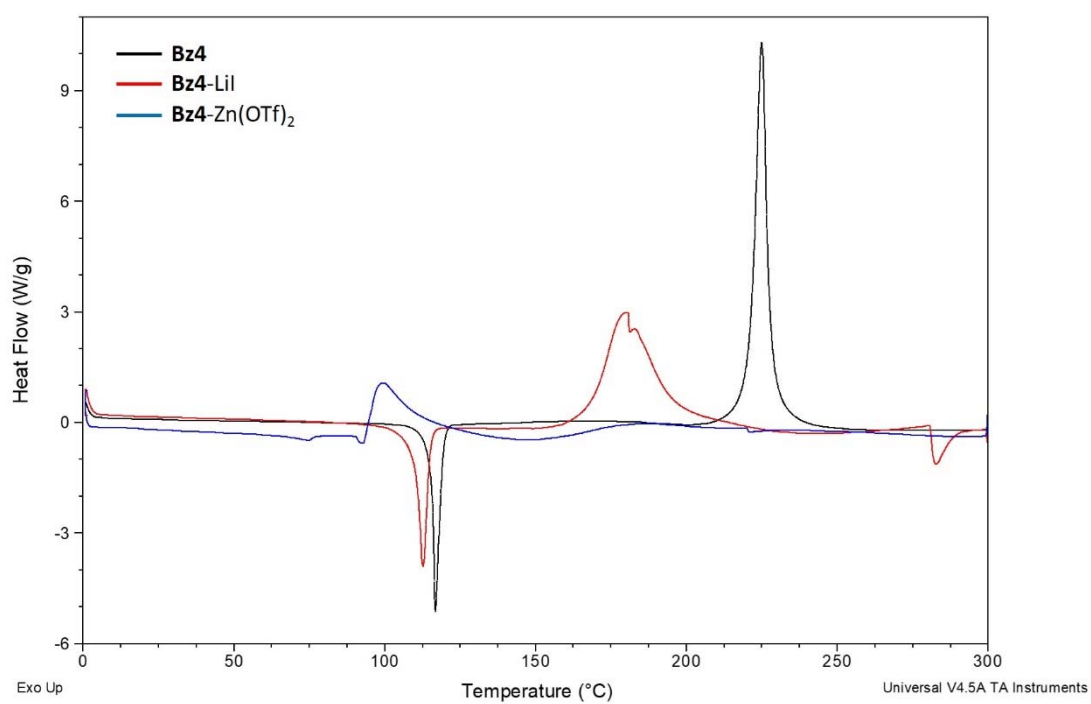


Fig. S15 DSC thermogram of neat **Bz4** and **Bz4**-catalyst systems.

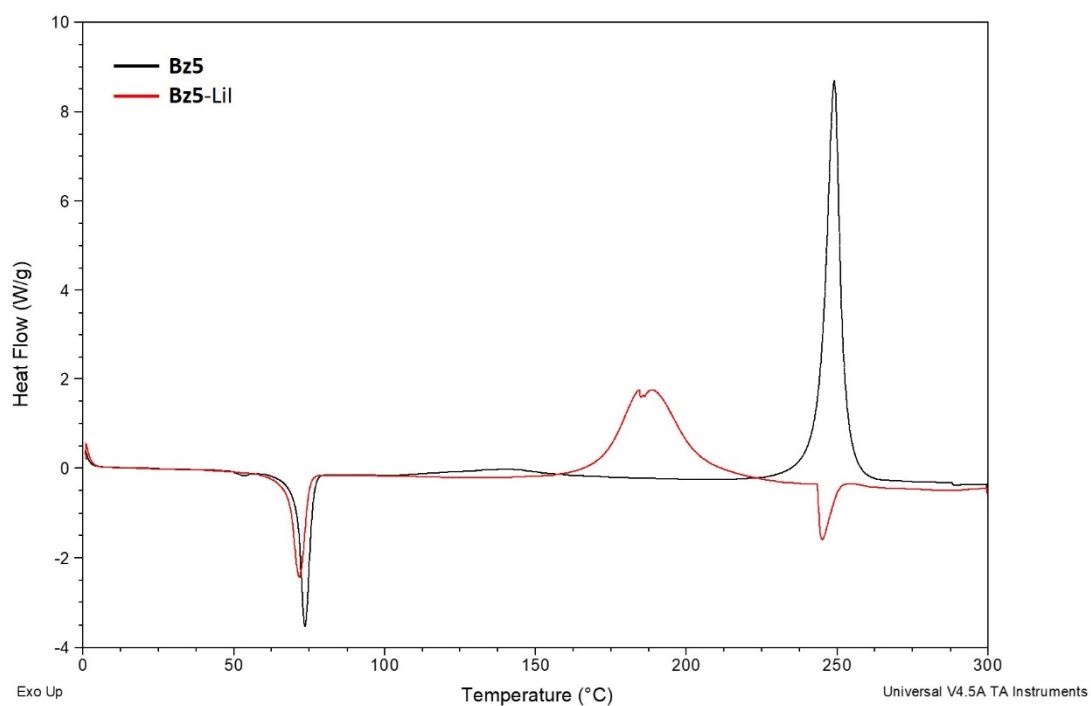


Fig. S16 DSC thermogram of neat **Bz5** and **Bz5**-catalyst systems.

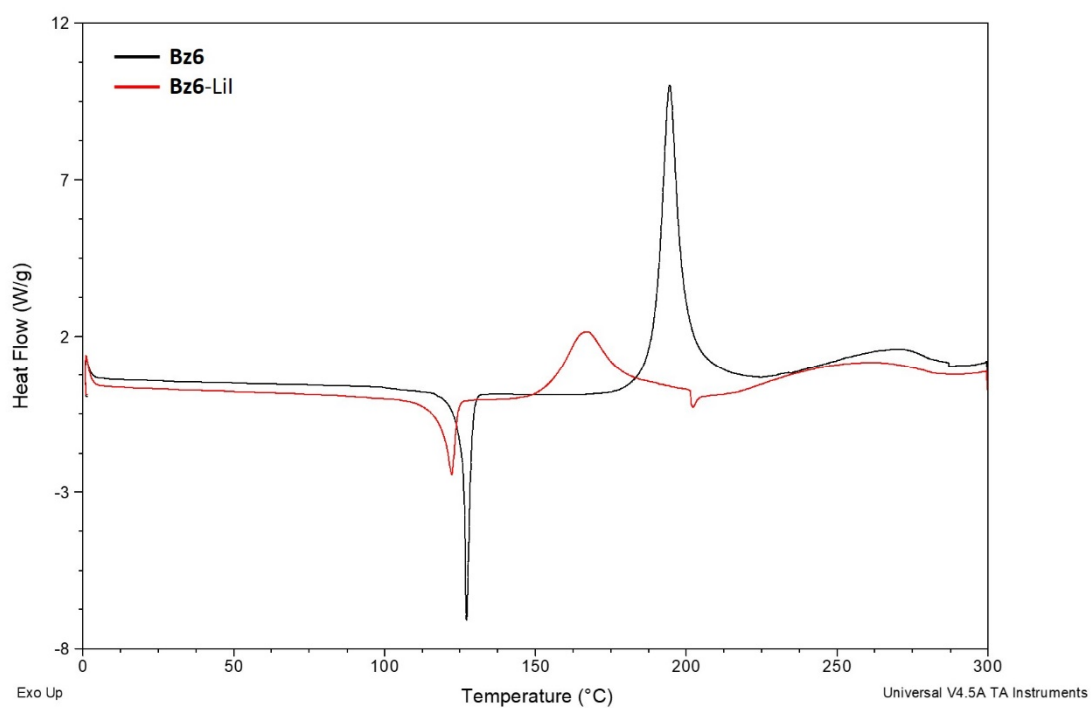


Fig. S17 DSC thermogram of neat **Bz6** and **Bz6**-catalyst systems.

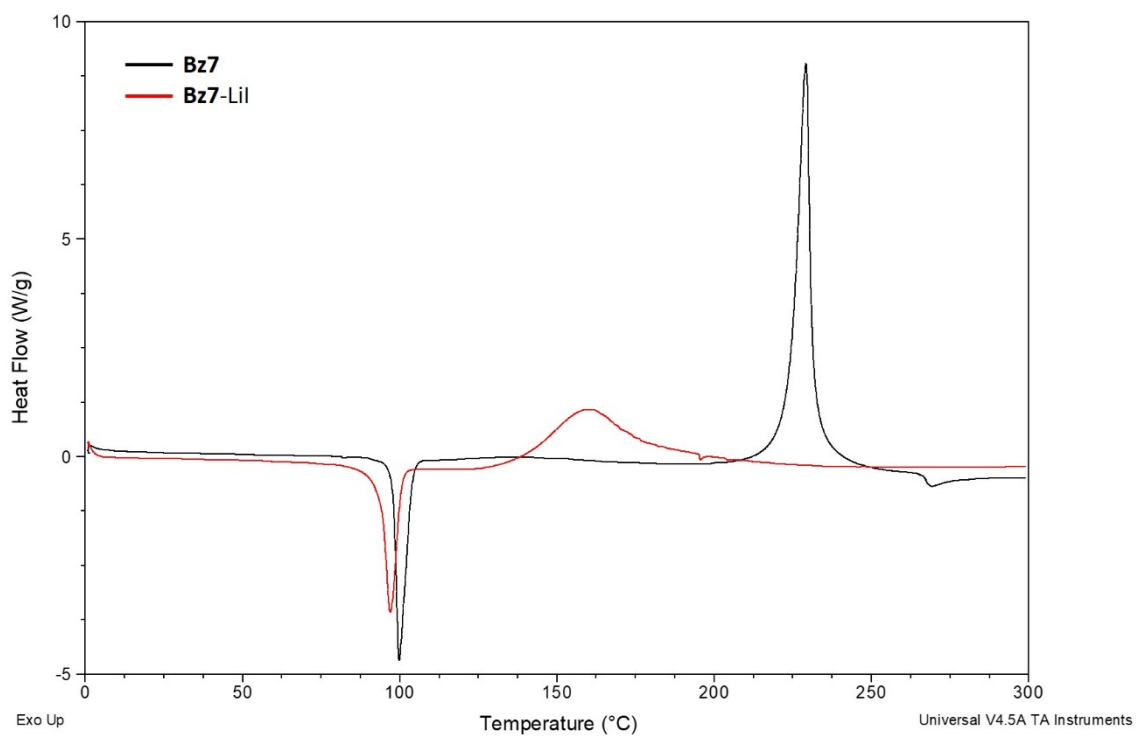


Fig. S18 DSC thermogram of neat **Bz7** and **Bz7**-catalyst systems.

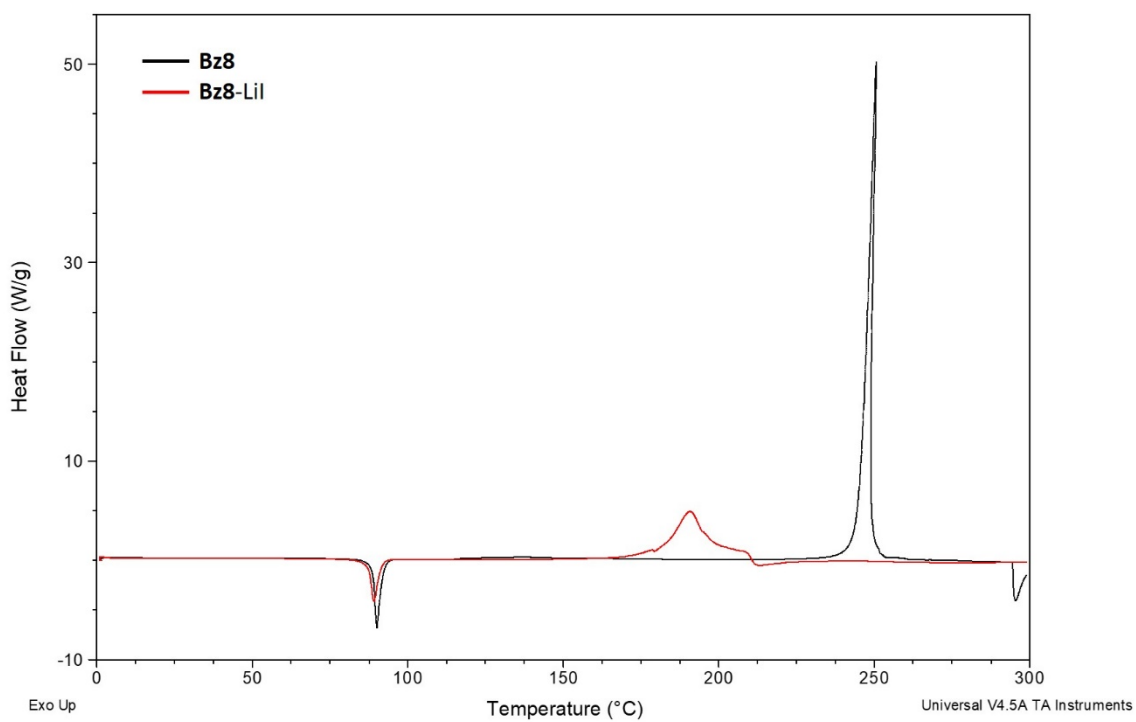


Fig. S19 DSC thermogram of neat **Bz8** and **Bz8**-catalyst systems.

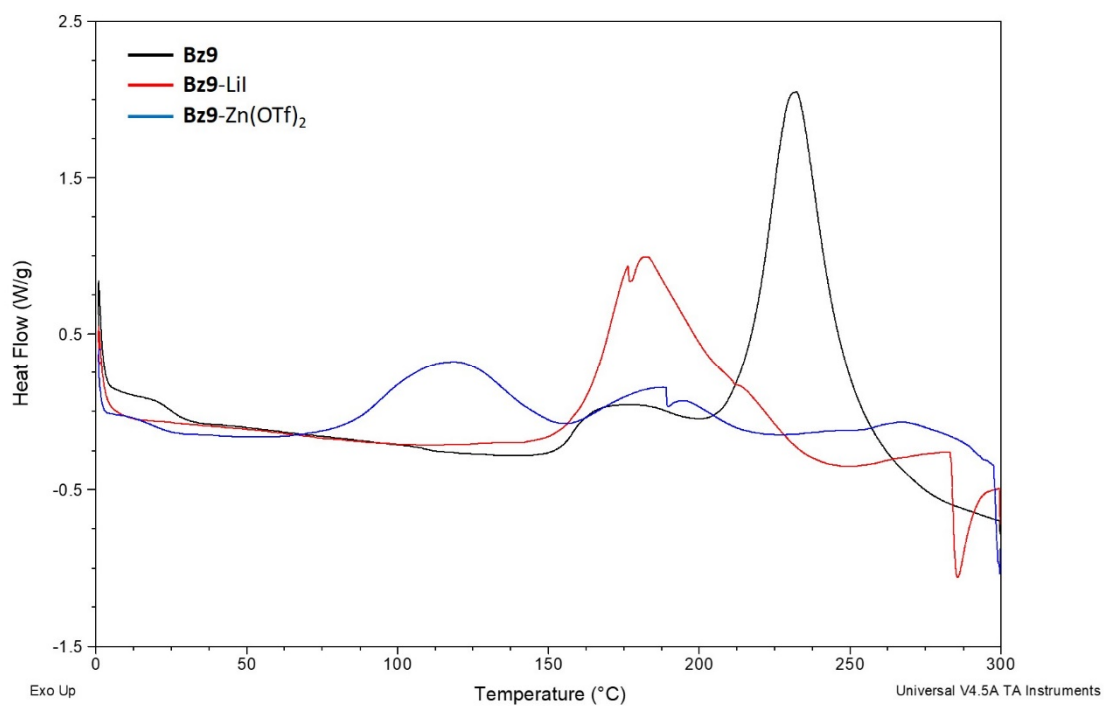


Fig. S20 DSC thermogram of neat **Bz9** and **Bz9**-catalyst systems.

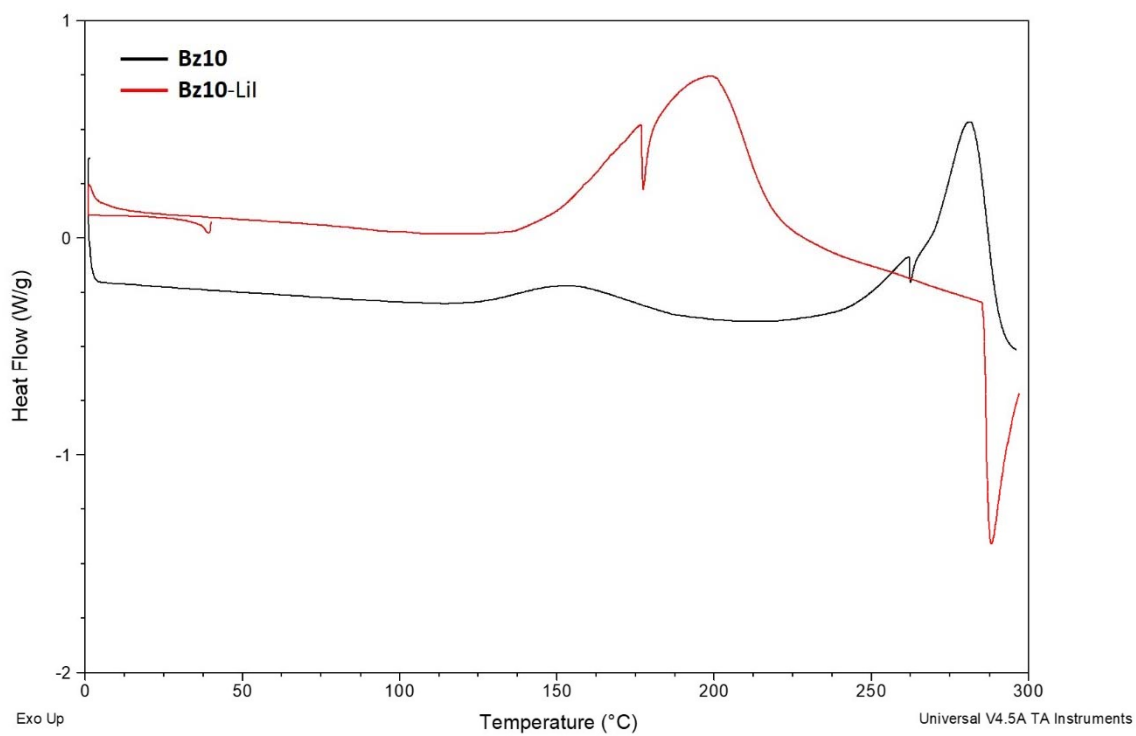


Fig. S21 DSC thermogram of neat **Bz10** and **Bz10**-catalyst systems.

4.4. Photothermal polymerization

General procedure: Each of the neat Bz monomers or monomer-catalyst systems (prepared as described in section 4.1) were placed either within a glass cuvette (50 x 0.8 x 0.4 mm) for solid samples (**Bz1**, **Bz2** and **Bz4-Bz9**, 0.2 – 0.3 g) (Fig. S22a) or within a glass vial ($\varnothing = 1$ cm) for liquid samples (**Bz3** and **Bz10**, 0.5 mL) (Fig. S22b). Then, they were irradiated with a pulsed green laser under ambient conditions for the required time (Fig. S22c).

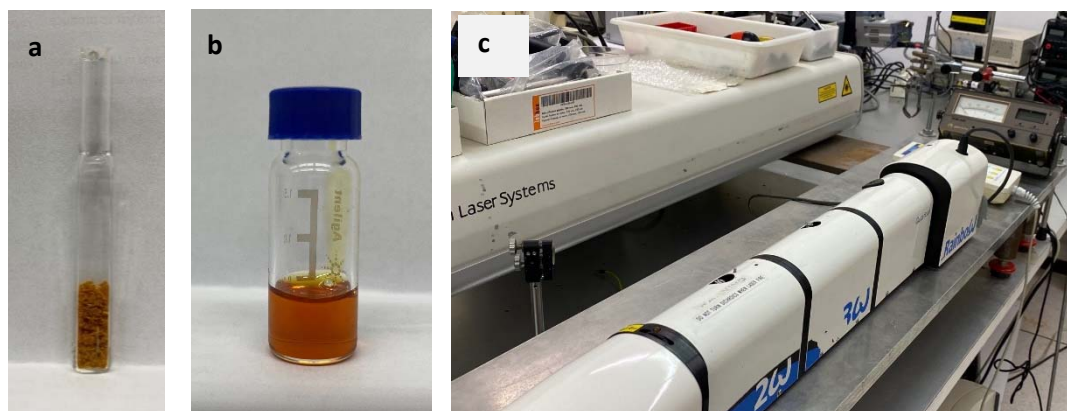


Fig. S22 (a) Solid and (b) liquid samples used in the photothermal polymerization experiments, which were mainly conducted employing (c) the 2nd harmonic of a ns-pulsed Nd:YAG laser as an irradiation source.

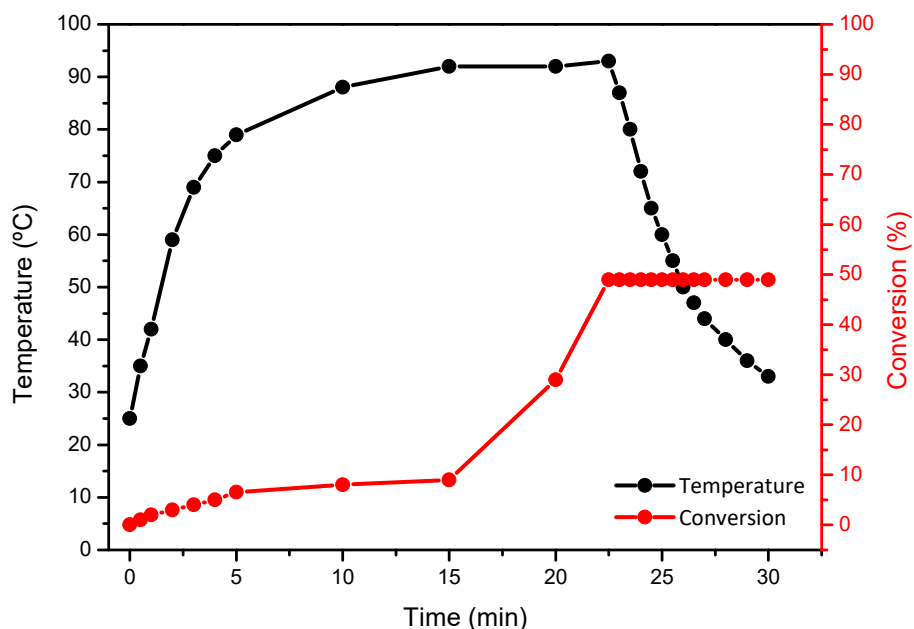


Fig. S23 Evolution of the reaction mixture temperature and monomer conversion during visible light irradiation of **Bz3**-LiI ($c_{\text{LiI}} = 15$ mol % relative to monomer concentration; $\lambda_{\text{exc}} = 532$ nm, power density = 1.1 W cm^{-2}). At $t_{\text{irr}} = 22.5$ min when ca. 50% of monomer conversion had been

reached, irradiation was stopped, which resulted in a sudden termination of the polymerization process and a more gradual decrease of temperature.

Frontal polymerization experiments: To investigate the self-propagation capacity of the photothermal polymerization process, frontal polymerization experiments were carried out. In these experiments, only a small region of the Bz-catalyst samples was irradiated to induce photopolymerization, while the monomer conversion was investigated for the nonirradiated area (Fig. S24).

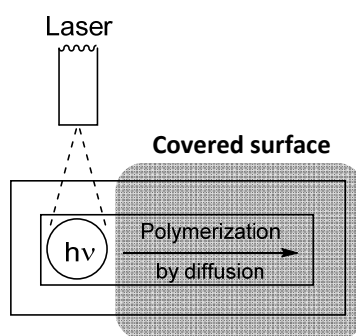


Fig. S24 Schematic representation of a frontal polymerization experiment. Pulsed laser irradiation of a specific area was conducted for 100 min ($\lambda_{\text{exc}} = 532 \text{ nm}$, $\varnothing_{\text{spot}} = 1 \text{ cm}$, power = 1.1 W cm^{-2}).

4.5. Chemical stability of Bz3-catalyst systems

Benzoxazine **Bz3** was mixed with Lil (15 mol % relative to monomer concentration) and $\text{Zn}(\text{OTf})_2$ (15 mol % relative to monomer content), respectively, in 2-3 mL of deuterated acetone. Both solutions were stirred for several days at room temperature. ^1H NMR analysis were performed every 24 h in order to check the intensity variation of benzoxazine peaks at $\delta \sim 5.4$ and 4.6 ppm .

5. Analysis of polybenzoxazines

5.1. Determination of the phenoxy-phenolic structure ratio

The phenoxy-phenolic structure ratio of photothermally polymerized PBz-catalyst samples^e and their annealed products was determined by a variation of the procedure developed in previous studies in our research group.^{7,8} The ¹H NMR signals located between $\delta \sim 4.0 - 6.0$ ppm and $3.5 - 4.0$ ppm were assigned to phenoxy-type CH₂ and phenolic-type CH₂ units, respectively. If m and n represent the signal integration of these phenoxy and phenolic CH₂ units, respectively, the phenoxy-to-phenolic ratio can be obtained as (in %): $[m/(m+n)] \cdot 100$ (Figs. S25-S28). Other typical signals found in the ¹H NMR spectra of polybenzoxazines are found at: (a) $\delta \sim 6.0 - 8.0$ ppm, which arise from the aromatic protons of the polymers; (b) $\delta \sim 8.0 - 9.5$ ppm, which are generally attributed to residual imine formation during the polymerization process.⁹

Thermal annealing of photothermally produced **PBz1-PBz4** was performed by heating up the corresponding polymers at 150 °C for 2 h. It must be noted that this resulted in the disappearance of most of the resonances in the $\delta \sim 4.0 - 6.0$ ppm region, thus indicating thermal phenoxy-to-phenolic conversion of the polymer structure.

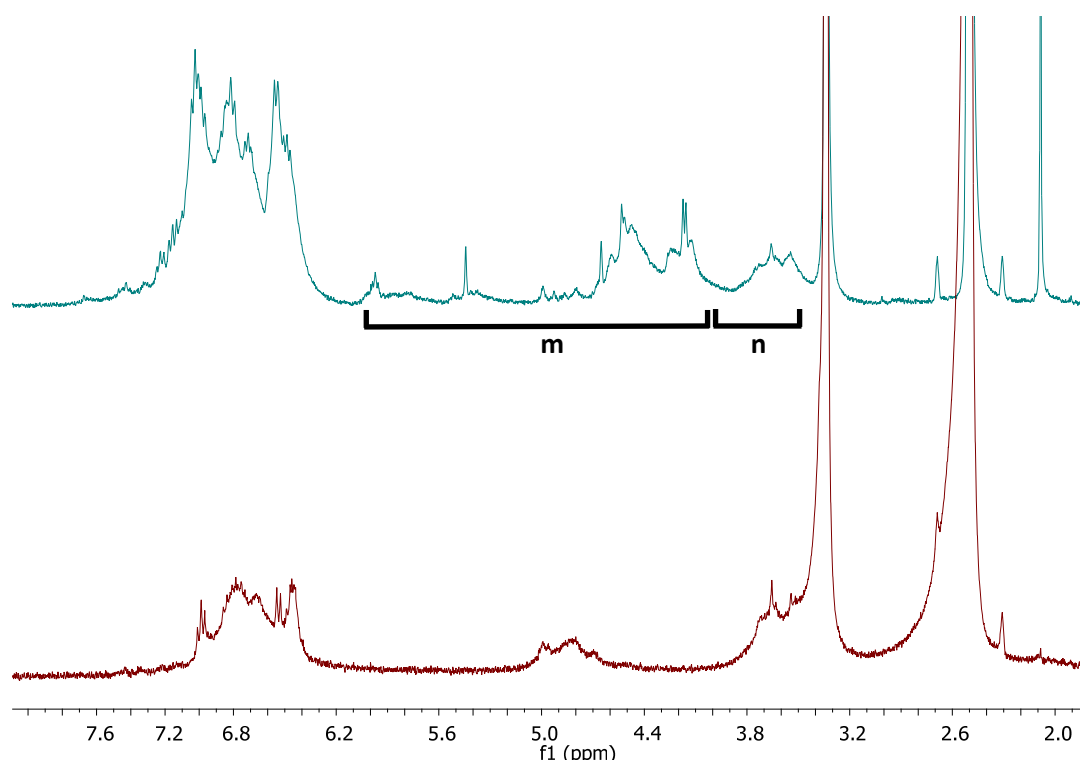


Fig. S25 ¹H NMR spectra (360 MHz, DMSO-*d*₆) of the PBz obtained by photothermal polymerization of **Bz1-LiI** (blue) and subsequent thermal annealing (red).

^e Phenoxy-phenolic structure ratio of the photothermally polymerized **Bz9-LiI** system and its annealed product could not be measured due to their poor solubility in all solvents.

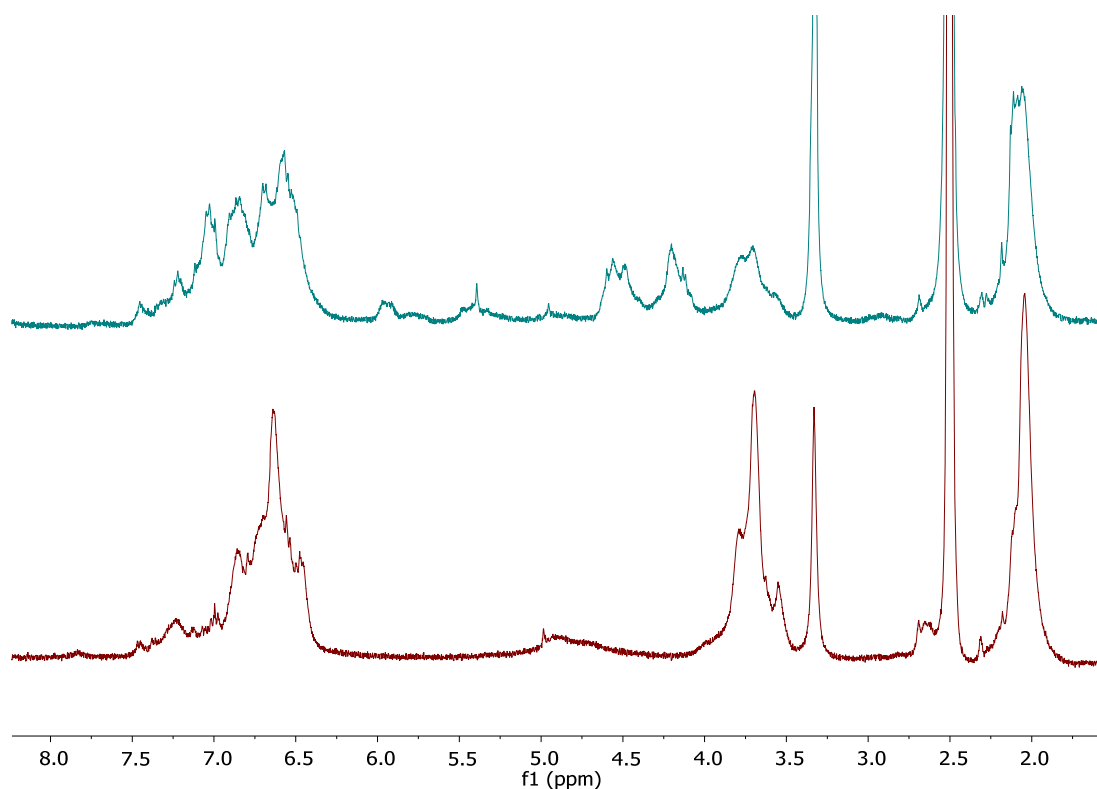


Fig. S26 ¹H NMR spectra (360 MHz, DMSO-*d*₆) of the PBz obtained by photothermal polymerization of **Bz2-LiI** (blue) and subsequent thermal annealing (red).

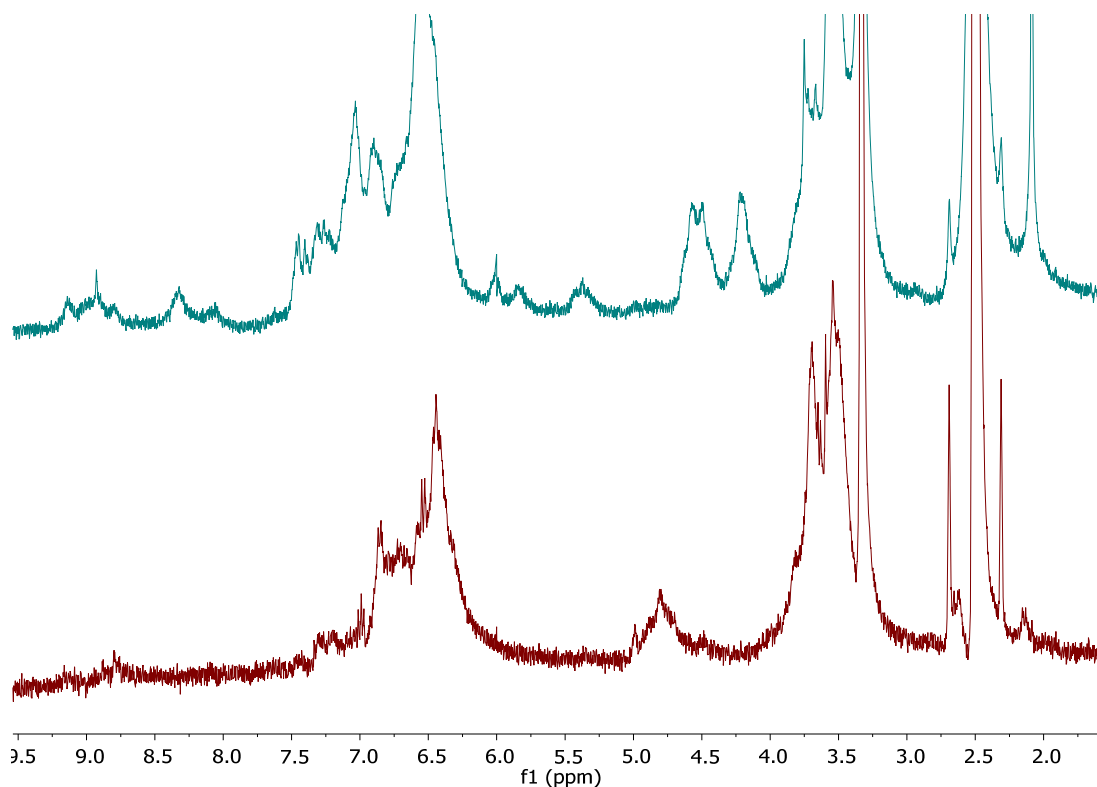


Fig. S27 ¹H NMR spectra (360 MHz, DMSO-*d*₆) of the PBz obtained by photothermal polymerization of **Bz3-LiI** (blue) and subsequent thermal annealing (red).

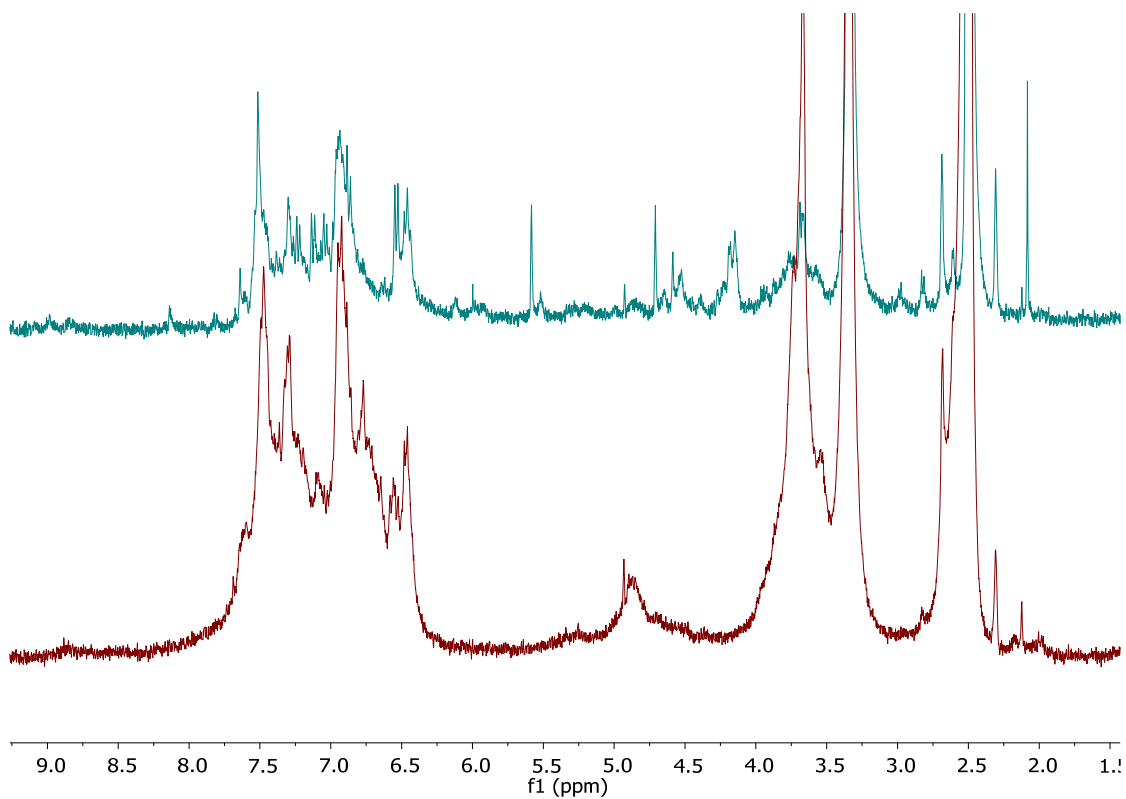


Fig. S28 ^1H NMR spectra (360 MHz, $\text{DMSO-}d_6$) of the PBz obtained by photothermal polymerization of **Bz4-LiI** (blue) and subsequent thermal annealing (red).

5.2. Determination of T_g

Transition glass temperatures of thermally-polymerized **PBz1-PBz4** and **PBz9** and photothermally-polymerized **PBz1-PBz4** and **PBz9** were measured by DSC analysis (Figs. S29-S33).

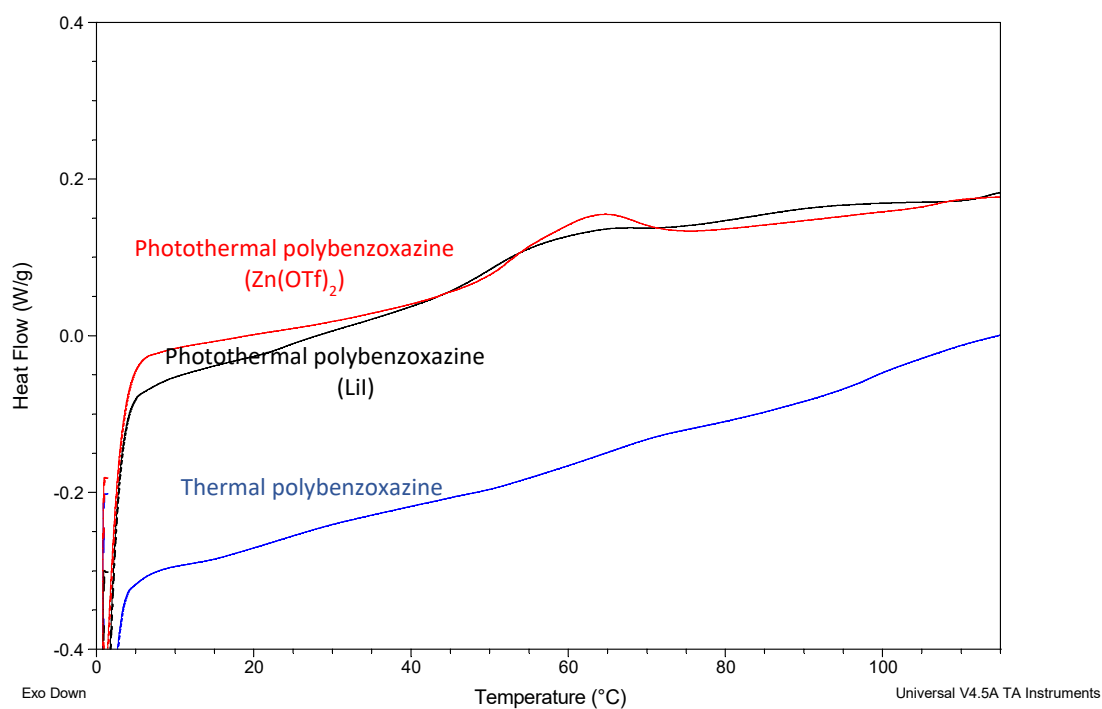


Fig. S29 DSC thermograms of the PBz materials obtained through the thermal (no catalyst) and photothermal polymerization of **Bz1**.

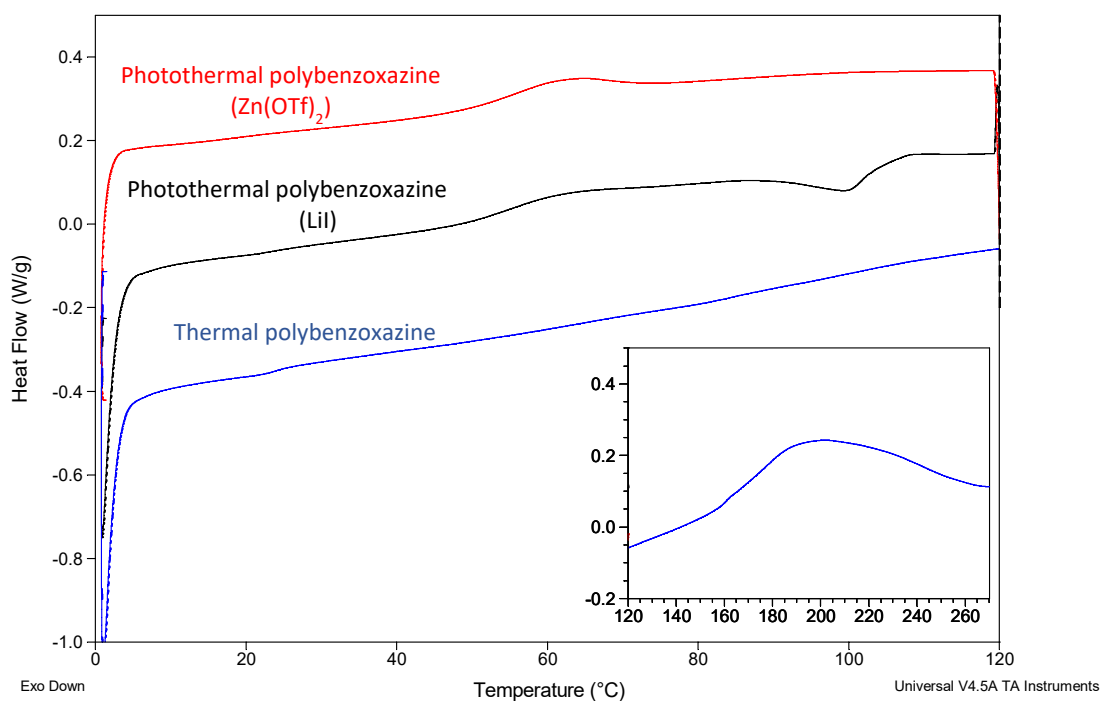


Fig. S30 DSC thermograms of the PBz materials obtained through the thermal (no catalyst) and photothermal polymerization of **Bz2**.

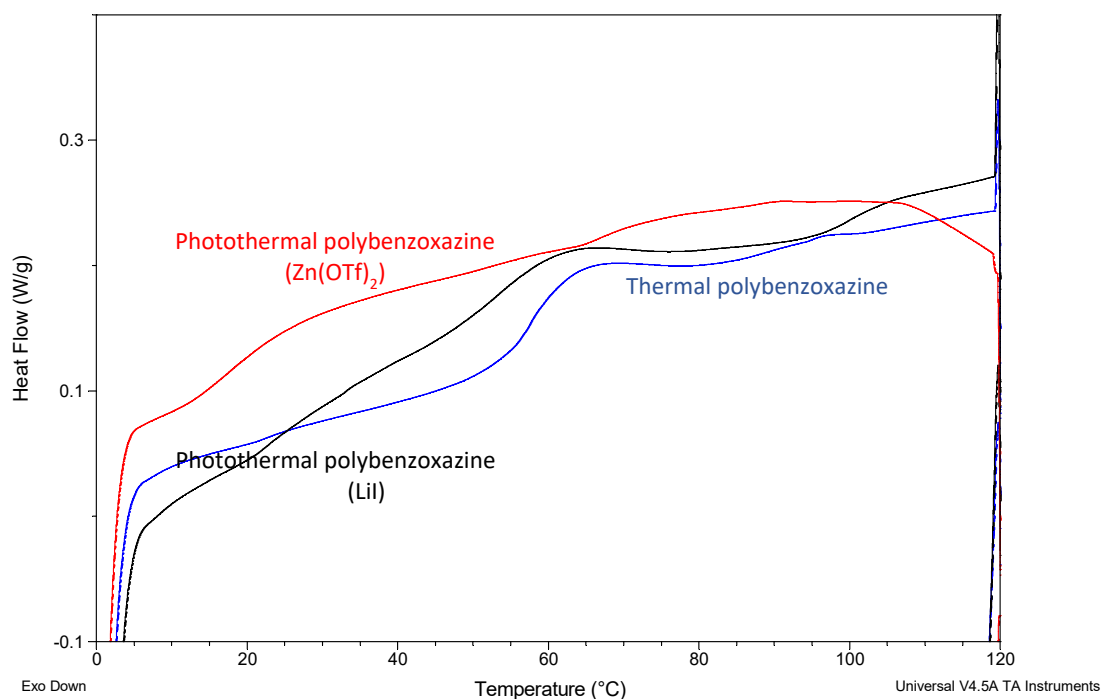


Fig. S31 DSC thermograms of the PBz materials obtained through the thermal (no catalyst) and photothermal polymerization of **Bz3**.

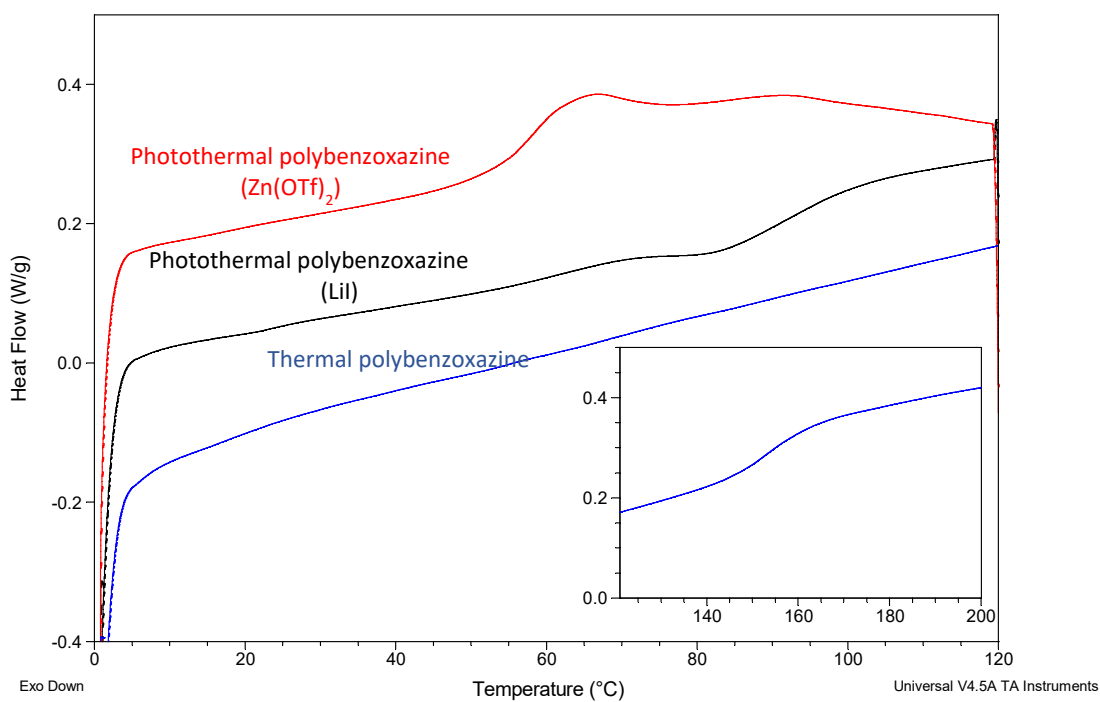


Fig. S32 DSC thermograms of the PBz materials obtained through the thermal (no catalyst) and photothermal polymerization of **Bz4**.

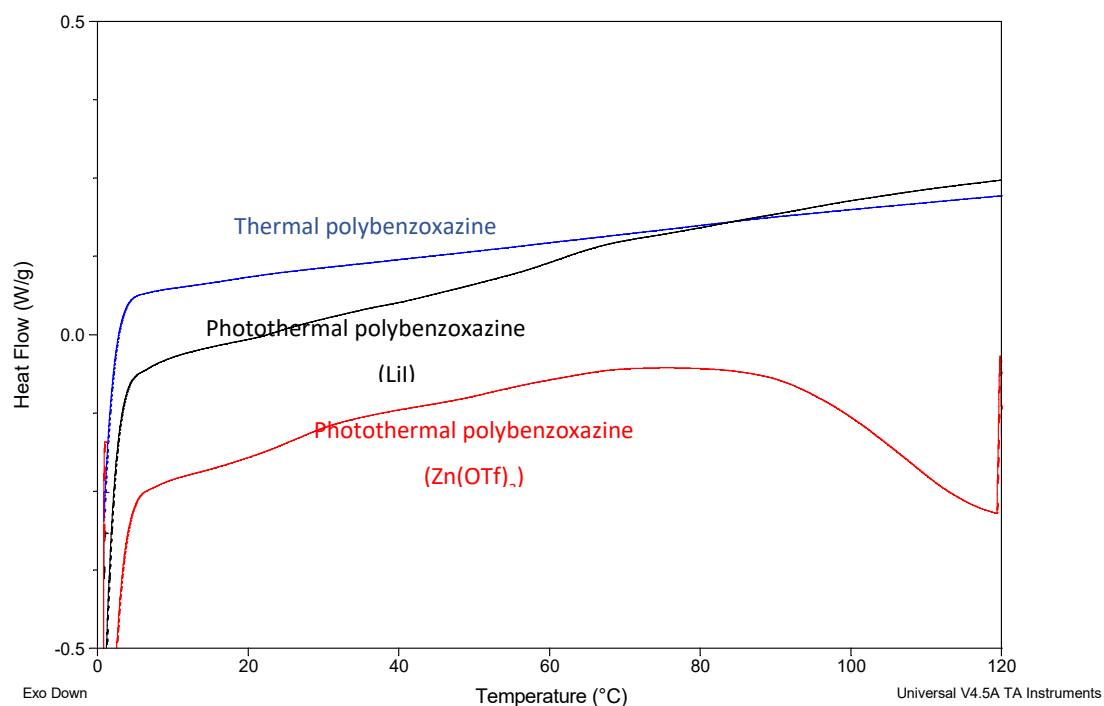


Fig. S33 DSC thermograms of the PBz materials obtained through the thermal (no catalyst) and photothermal polymerization of **Bz9**.

5.3. Determination of char yield and thermal decomposition

The char yields of thermally-polymerized **PBz1-PBz4** and **PBz9** and photothermally-polymerized **PBz1-PBz4** and **PBz9** were registered by thermogravimetric analysis (Figs. S34-S38). To assess the thermal stability of the polymers, we shown in Table S3 the temperatures for 5% and 10% weight loss determined from the TGA measurements.

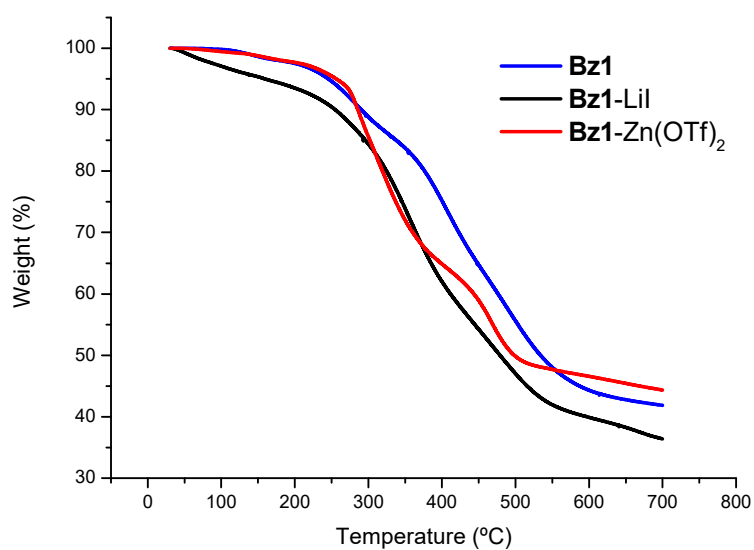


Fig. S34 TGA thermograms of the PBz materials obtained through the thermal (no catalyst) and photothermal polymerization of **Bz1**.

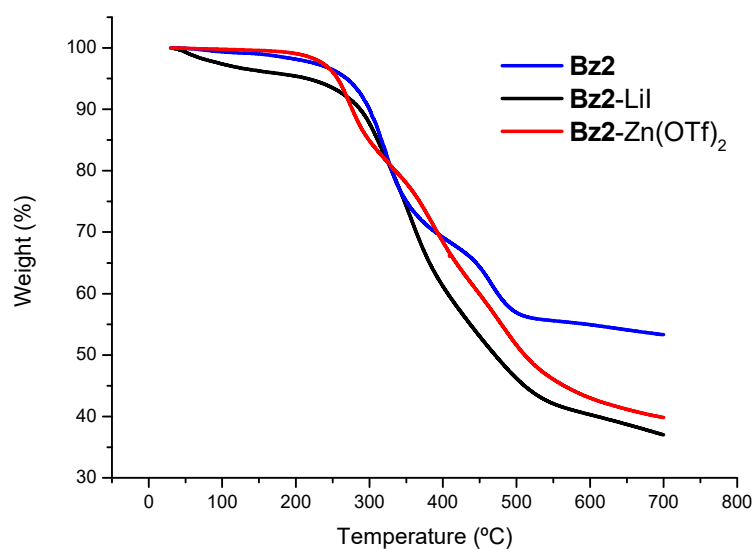


Fig. S35 TGA thermograms of the PBz materials obtained through the thermal (no catalyst) and photothermal polymerization of **Bz2**.

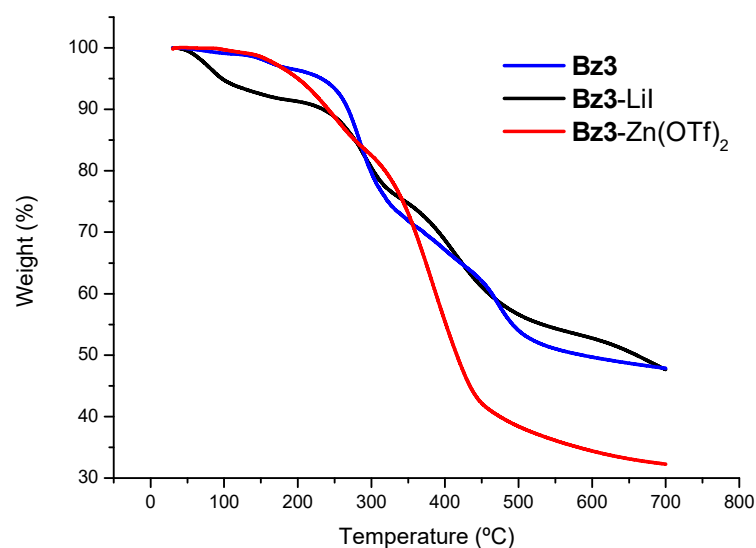


Fig. S36 TGA thermograms of the PBz materials obtained through the thermal (no catalyst) and photothermal polymerization of **Bz3**.

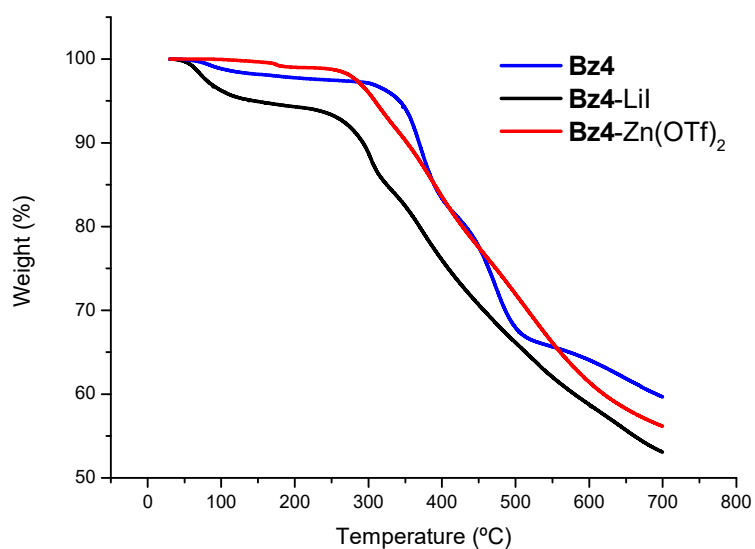


Fig. S37 TGA thermograms of the PBz materials obtained through the thermal (no catalyst) and photothermal polymerization of **Bz4**.

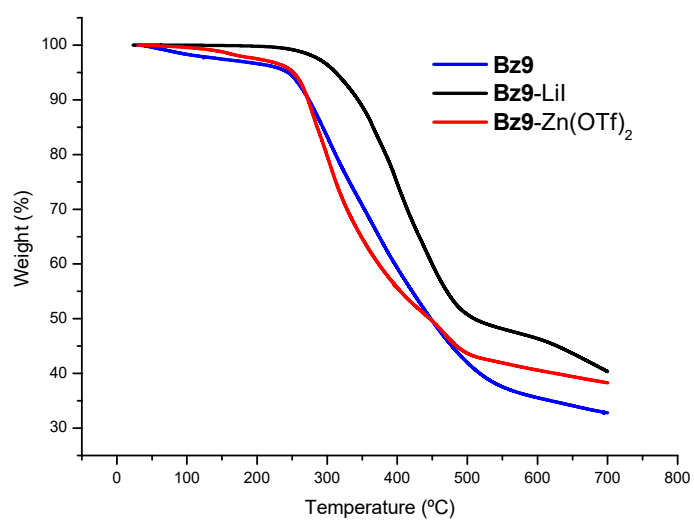


Fig. S38 TGA thermograms of the PBz materials obtained through the thermal (no catalyst) and photothermal polymerization of **Bz9**.

Table S4. T_{5%} and T_{10%} of neat thermal **PBz1-PBz4** and **PBz9** and their photothermal PBz-catalyst systems.

Bz	Catalyst	T _{5%} (°C)	T _{10%} (°C)
Bz1	-	246	290
	LiI	159	255
	Zn(OTf) ₂	256	286
Bz2	-	257	277
	LiI	216	288
	Zn(OTf) ₂	269	300
Bz3	-	232	269
	LiI	97	234
	Zn(OTf) ₂	200	241
Bz4	-	342	369
	LiI	145	293
	Zn(OTf) ₂	309	353
Bz9	-	312	344
	LiI	244	274
	Zn(OTf) ₂	252	273

5.4. Determination of gel content

The gel content of selected photothermally- and thermally-prepared polymers was determined as previously reported by us.¹⁰ About 0.7 g of the polymer material of interest were subjected to a 24 h Soxhlet extraction using acetone as a solvent. This led to dissolution of linear polymer chains, leaving behind the insoluble cross-linked 3D network. Therefore, comparison of the final insoluble material left in the cellulose cartridge used in the extraction (m_{gel}) with the initial polymer mass (m_0) allowed us the calculation of the gel content using equation (3):

$$Gel\ content\ (\%) = \frac{m_{gel}}{m_0} \cdot 100 \quad (3)$$

5.5. Purification of polymer-catalyst samples

To explore the purification of polymer-catalyst samples, we selected the polymer material obtained from the photopolymerization of the **Bz3**-Zn(OTf)₂ system ($C_{Zn(OTf)_2}$ = 15 mol %) as a

benchmark case. About 0.5 g of this material were suspended within 5 mL of cold acetone and the resulting mixture was stirred for 4 h in an ice bath. After this time, most of the initial polymer had been dissolved, which was separated from the remaining solid by filtration. After solvent evaporation of the filtrate, the dissolved polymer was analyzed by ^1H NMR and ^{19}F NMR in $\text{DMSO-}d_6$ and the obtained spectra were compared with those registered before purification. In the case of ^{19}F NMR, a controlled quantity of trifluoroacetic acid (10 μL) was added as an internal standard to quantify the decrease in the integral of the signal corresponding to the triflate anions after purification.

6. Photolithography experiments

Photolithography experiments were performed with a NEJE Master 2/2s laser-engraving machine equipped with a focusable 405 nm cw laser (33 W cm^{-2}) and the NEJE v5.6 software (Fig. S39). Samples were prepared by depositing a **Bz3/Bz9**-Zn(OTf)₂ formulation onto a glass substrate (9:1 **Bz3**:**Bz9** ratio, $c_{\text{catalyst}} = 15 \text{ mol \%}$ relative to the total monomer content), which was then subjected to photolithography experiments. To remove the excess of unreacted monomer-catalyst system, the samples were gently rinsed with an organic solvent (e.g., ethyl acetate).

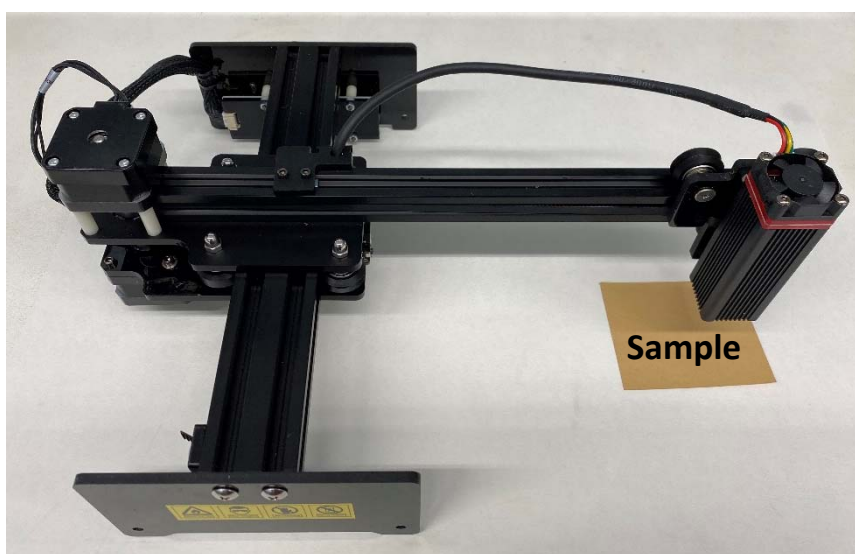


Fig. S39 Image of the laser-engraving machine used for the photolithography experiments.

7. NMR spectra

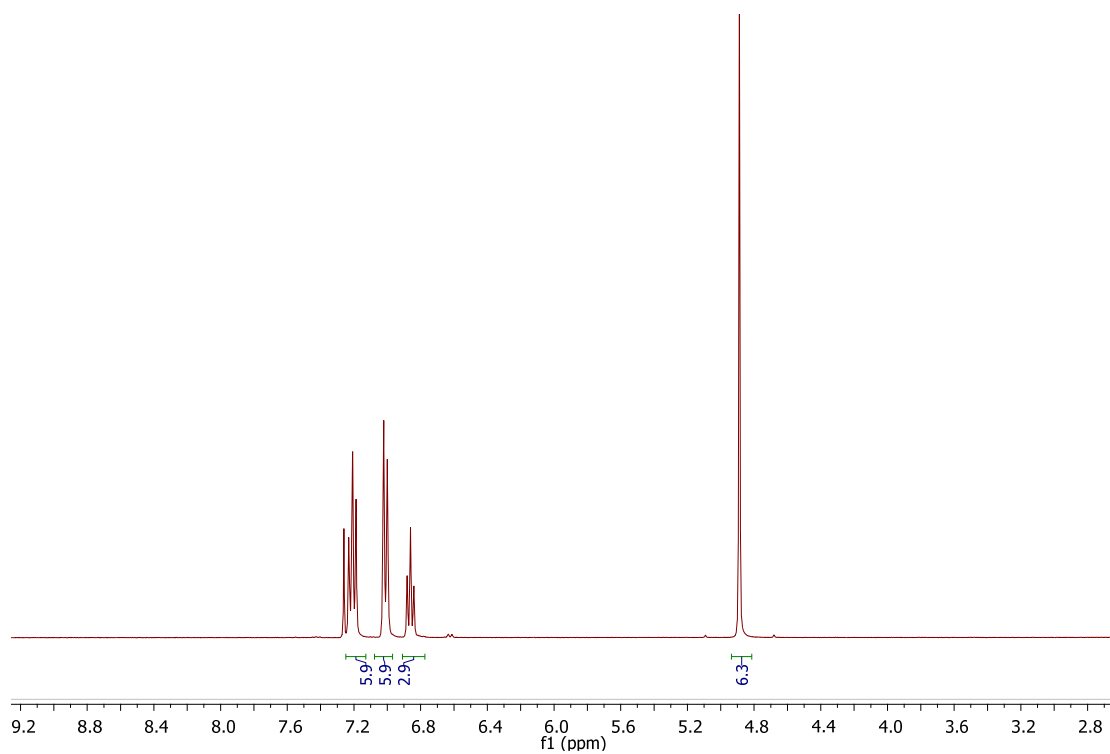


Fig. S40 ^1H NMR spectrum (360 MHz, CDCl_3) of 1,3,5-triphenyltriazine (**3**).

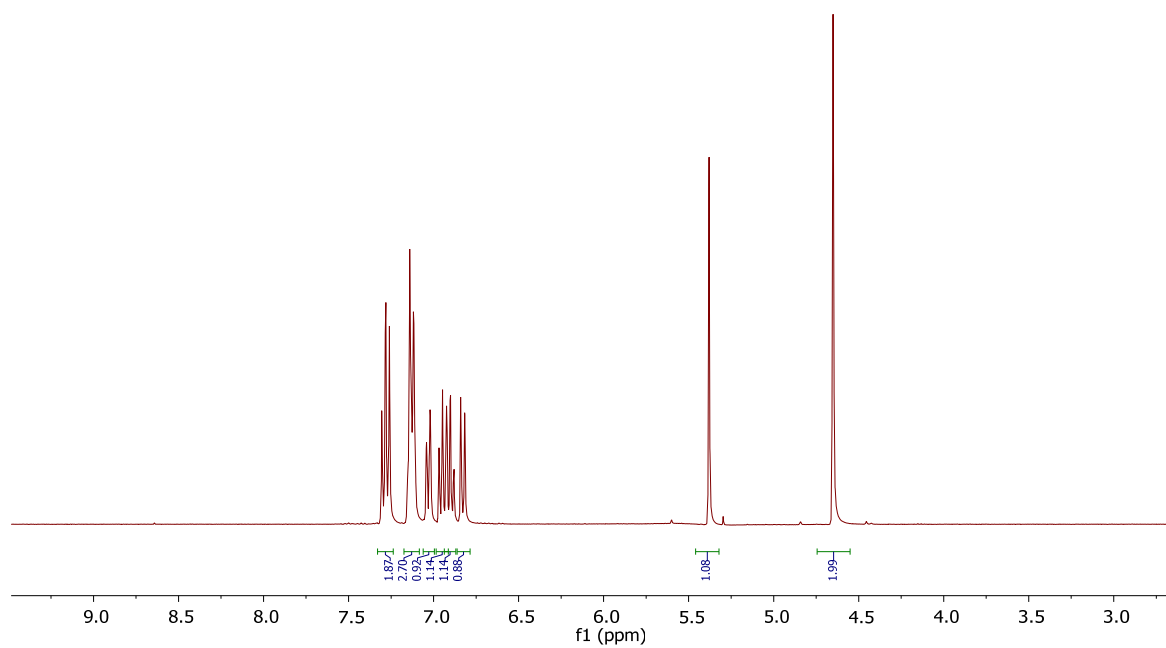


Fig. S41 ¹H NMR spectrum (360 MHz, CDCl₃) of **Bz1**.

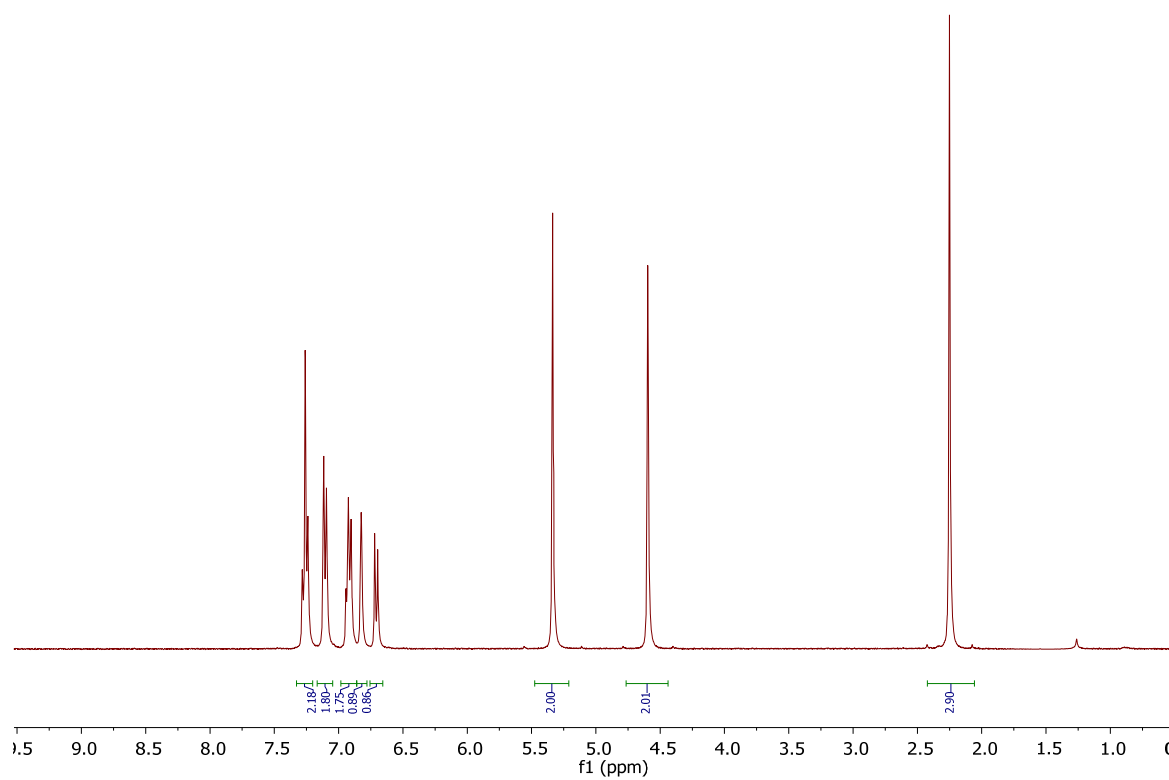


Fig. S42 ¹H NMR spectrum (360 MHz, CDCl₃) of **Bz2**.

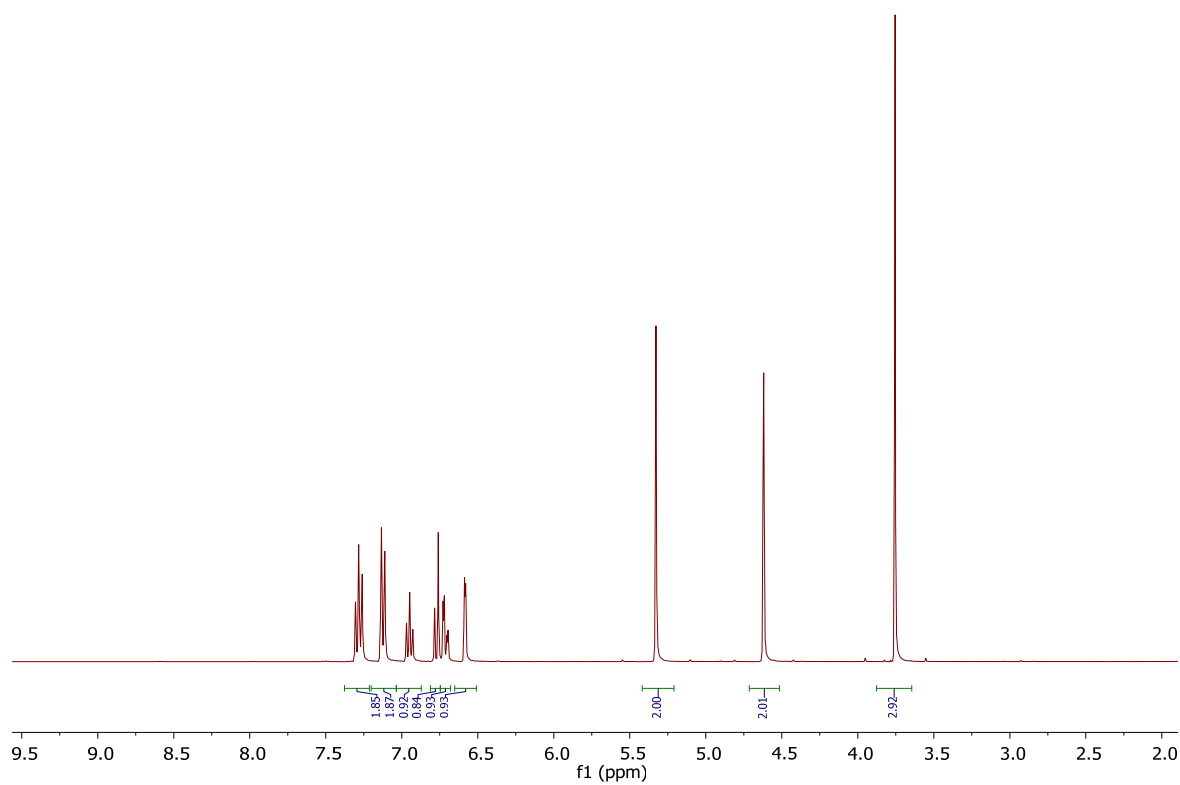


Fig. S43 ¹H NMR spectrum (360 MHz, CDCl₃) of **Bz3**.

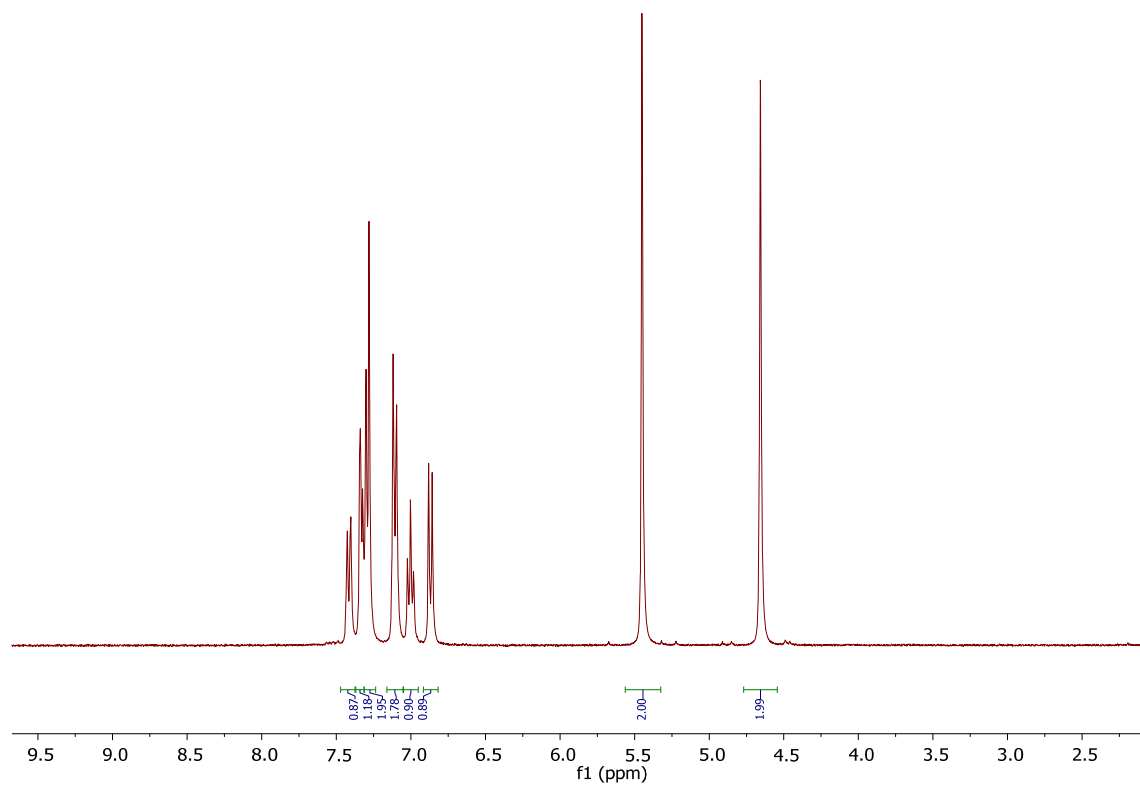


Fig. S44 ¹H NMR spectrum (360 MHz, CDCl₃) of **Bz4**.

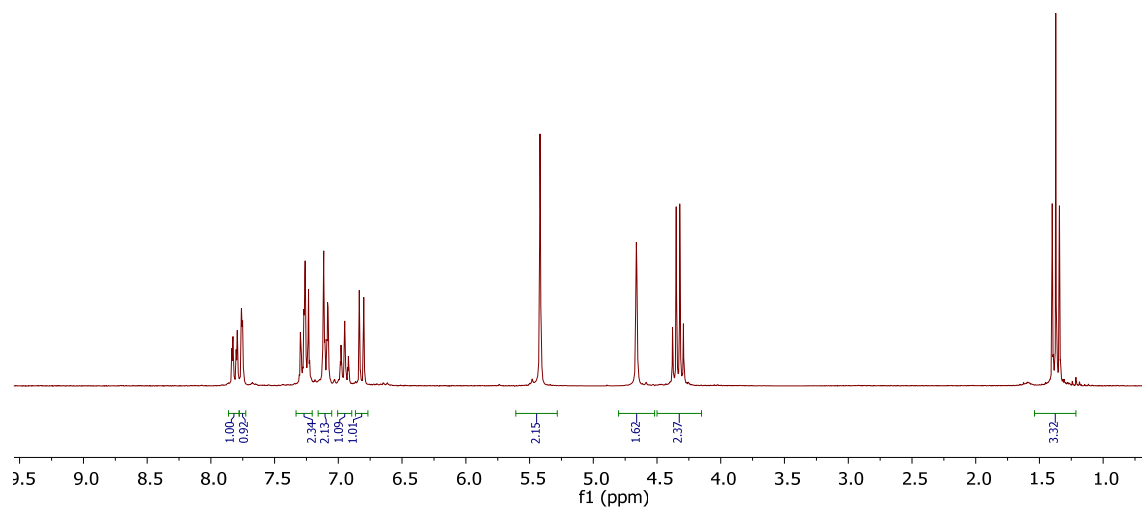


Fig. S45 ^1H NMR spectrum (360 MHz, CDCl_3) of **Bz5**.

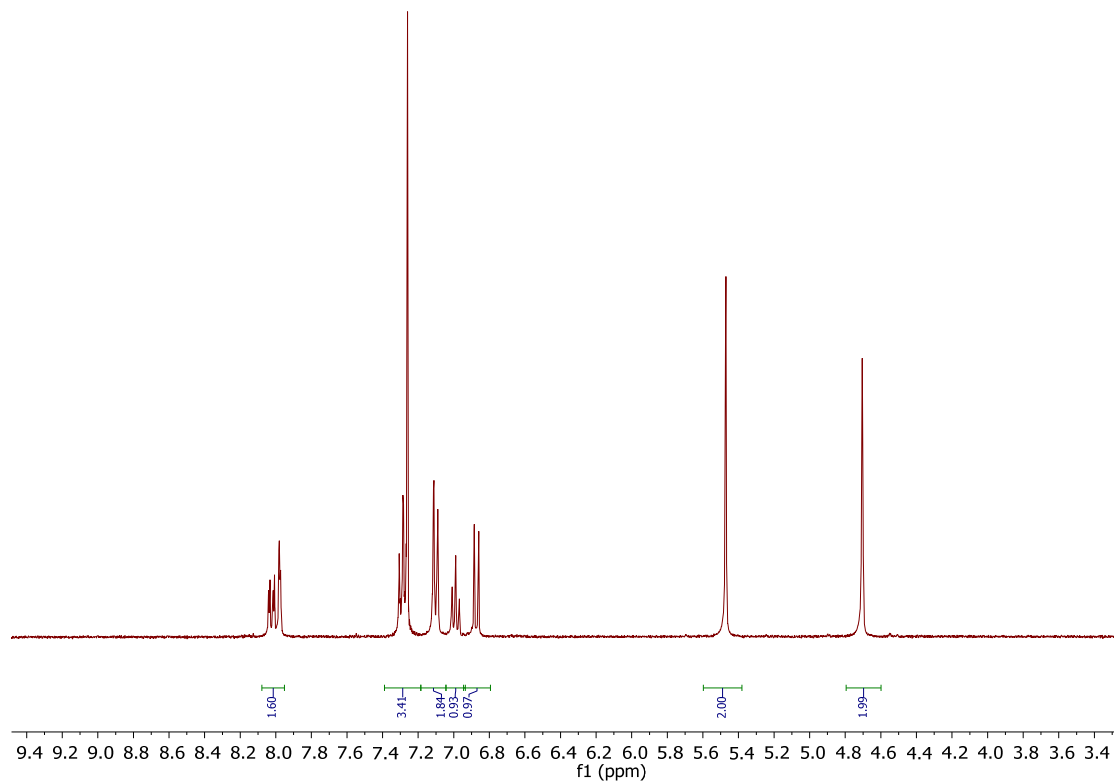


Fig. S46 ^1H NMR spectrum (360 MHz, CDCl_3) of **Bz6**.

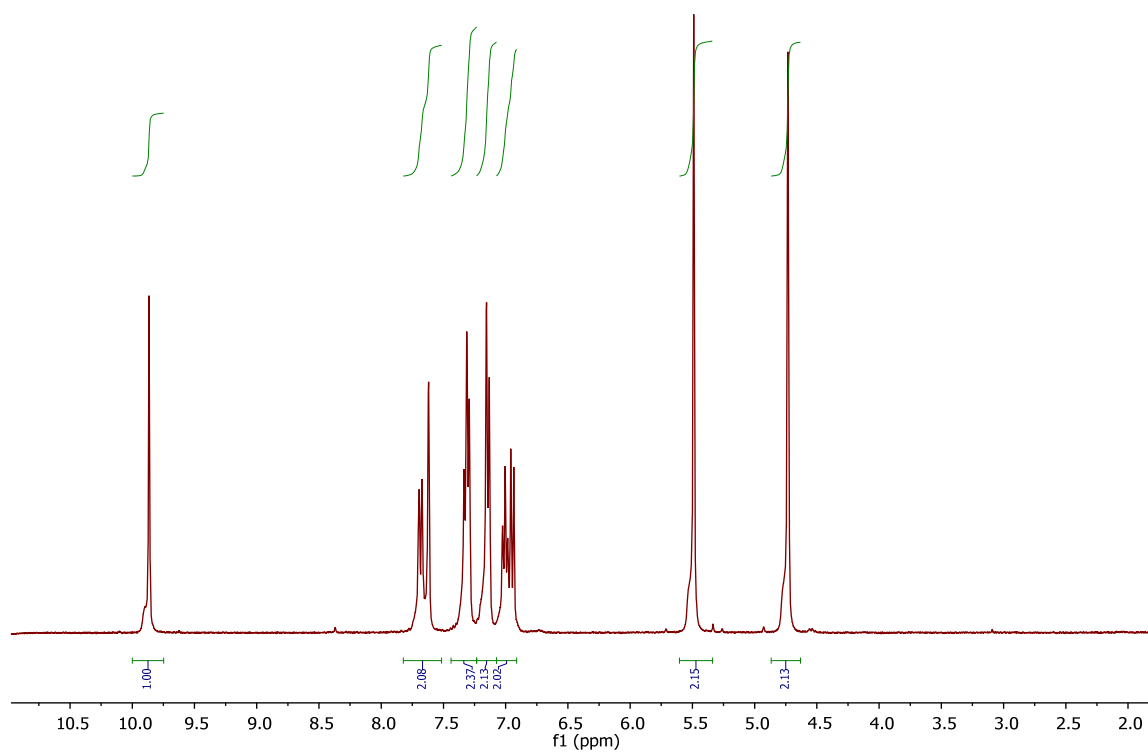


Fig. S47 ¹H NMR spectrum (250 MHz, CDCl₃) of **Bz7**.

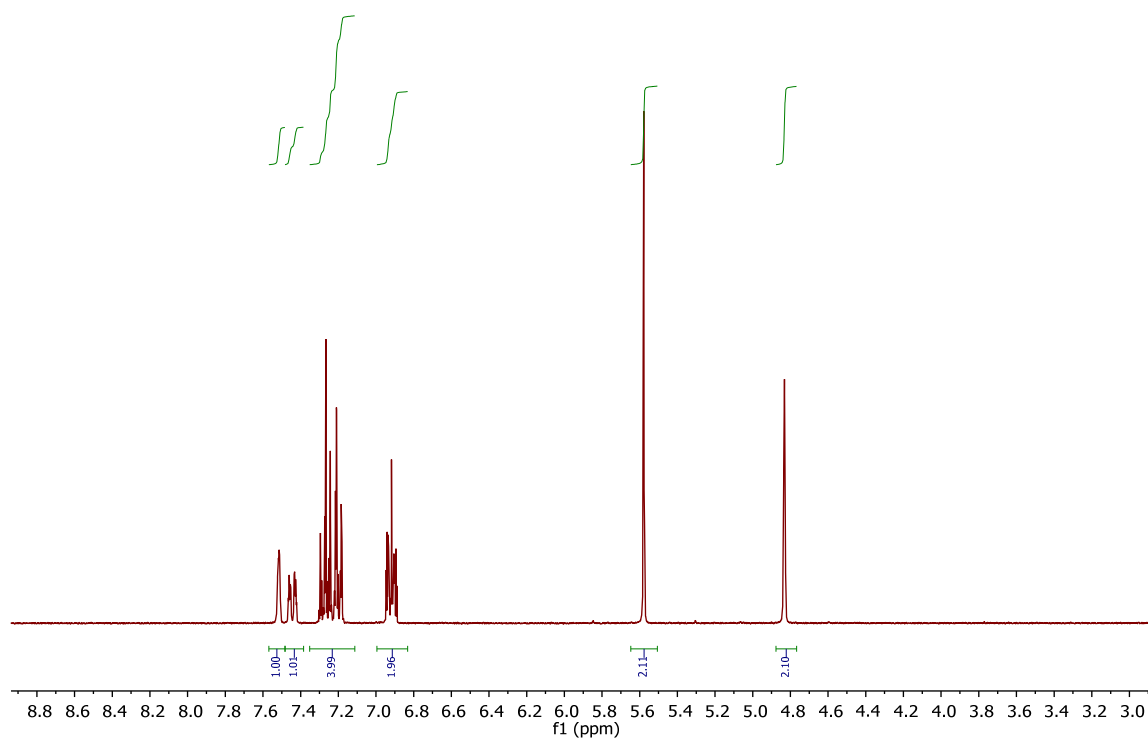


Fig. S48 ¹H NMR spectrum (300 MHz, (CD₃)₂CO) of **Bz8**.

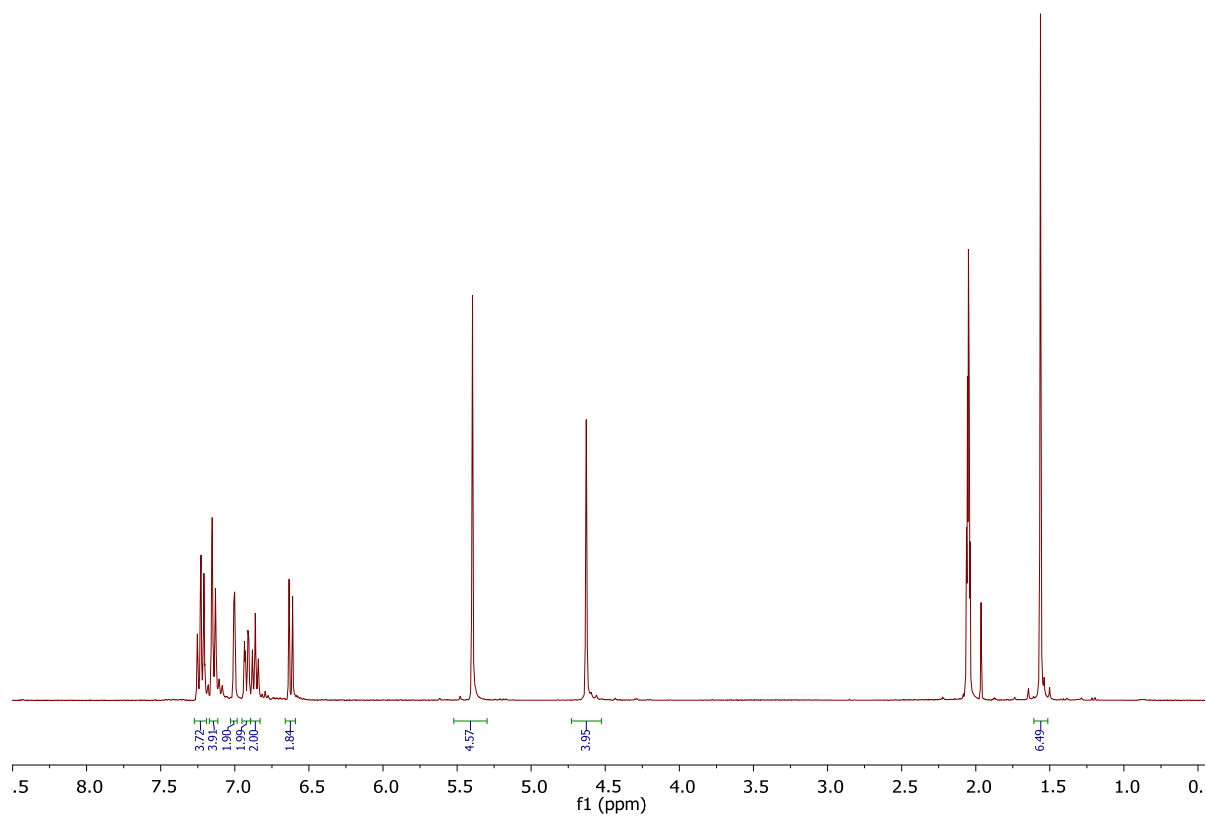


Fig. S49 ^1H NMR spectrum (360 MHz, CDCl_3) of **Bz9**.

8. References

- ¹ R. Andreu, J. A. Reina and J. C. Ronda, *J. Polym. Sci. A: Polym. Chem.*, 2008, **46**, 3353-3366.
- ² M. A. Espinosa, V. Cádiz and M. Galia, *J. Appl. Polym. Sci.*, 2003, **90**, 470-481.
- ³ J. Salabert, R. M. Sebastián and J. Marquet. *Macromolecules*, 2018, **51**, 3672-3679.
- ⁴ A. Martos, R. M. Sebastián and J. Marquet. *Eur. Polym. J.* 2018, **108**, 20-27.
- ⁵ H. M. Ma, Y. Liu, Y. X. Liu, J. J. Qiu and C. Liu, *RSC Adv.*, 2015, **5**, 102441-102447.
- ⁶ P. Chutayothin and H. Ishida, *Macromolecules*, 2010, **43**, 4562-4572.
- ⁷ C. Liu, D. Shen, R. M. Sebastián, J. Marquet and R. Schönfeld, *Polymer*, 2013, **54**, 2873-2878.
- ⁸ C. Liu, D. Shen, R. M. Sebastián, J. Marquet and R. Schönfeld. *Macromolecules*, 2011, **44**, 4616-4622.
- ⁹ P. Chutayothin and H. Ishida, *Macromolecules*, 2010, **43**, 4562-4572.
- ¹⁰ A. Martos, M. Soto, H. Schäfer, K. Koschek, J. Marquet and R. M. Sebastián, *Polymers*, 2020, **12**, 254.